Two experiments using brain imaging to answer questions about the neural basis of Human Vision

By

Arjun Mukerji

A dissertation submitted in partial satisfaction of the

requirements for the degree of

Doctor of Philosophy

in

Neuroscience

in the

Graduate Division

of the

University of California, Berkeley

Committee in charge:

Professor Michael A. Silver, Chair
Professor Dennis M. Levi
Professor William J. Jagust
Professor Jack L. Gallant

Fall 2022

Abstract

Two experiments using brain imaging to answer questions about the neural basis of Human Vision

by

Arjun Mukerji

Doctor of Philosophy in Neuroscience

University of California, Berkeley

Professor Michael A. Silver, Chair

Anatomical, physiological, and psychophysical approaches have revealed a great deal about the structure and function of the visual system. Non-invasive techniques based on nuclear magnetic resonance supplement these approaches by allowing the possibility of recording from the awake, behaving human brain. Here, we present two experiments using different non-invasive techniques to answer questions about the neural basis of human vision.

In Chapter 2, we examine the relationship between γ-aminobutyric acid (GABA), perceptual suppression, and amblyopia ("lazy eye"). In amblyopia, abnormal visual experience during development leads to an enduring loss of visual acuity in adulthood. Physiological studies in animal models suggest that intracortical GABAergic inhibition may mediate visual deficits in amblyopia. To better understand the relationship between visual cortical GABA and perceptual suppression in persons with amblyopia (PWA), we employed magnetic resonance spectroscopy (MRS) to quantify GABA levels in both PWA and normally-sighted persons (NSP). In the same individuals, we obtained psychophysical measures of perceptual suppression for a variety of ocular configurations. In PWA, we found a robust negative correlation between the depth of amblyopia (the difference in visual acuity between the amblyopic and non-amblyopic eyes) and GABA concentration that was specific to visual cortex and was not observed in a sensorimotor cortical control region. Moreover, lower levels of visual cortical GABA were associated with weaker perceptual suppression of the fellow eye by the amblyopic eye and stronger suppression of the amblyopic eye by the fellow eye. Taken together, our findings provide evidence that intracortical GABAergic inhibition is an important component of the pathology of human amblyopia and suggest possible therapeutic interventions to restore vision in the amblyopic eye through enhancement of visual cortical GABAergic signaling in PWA.

In Chapter 3, we use functional magnetic resonance imaging (fMRI) to identify cortical and subcortical components of the visual system. In particular, we localized many topographically-organized visual cortical areas as well as the lateral geniculate nucleus (LGN) and the magnocellular and parvocellular subdivisions thereof. We report the extension of this M/P localization procedure to fMRI data acquired with multiband

acceleration. We also examined thalamocortical coupling between the LGN subdivisions and visual cortical areas but found no effects of stimulus type or spatial attention.

Table of contents

Acknowledgments

This dissertation would not have been possible without a lot of help.

First, I would like to thank Michael for his patience and support over the years. Thank you for teaching me how to be a better scientist and person. Your acumen as a researcher is only matched by the unfailingly positive way you treat others, and both are inspirations to me.

I'm grateful to have worked alongside many impressive and supportive labmates. Special thanks to Eunice Yang, Dev Vartak, and Kelly Byrne, whose work appears in this dissertation. To everyone in the Silver lab, past and present, thank you for your guidance over the years.

Thank you to the entire Helen Wills community. I feel lucky to have met many brilliant people who helped me broaden my horizons. Thank you to Candace Groskreutz, who was the HWNI program administrator for most of my time at Cal. Thank you to the members of my thesis committee for their advice and feedback: Dennis Levi, Bill Jagust, and Jack Gallant.

Special thanks to my partner Laura, without whose love and support I doubt I'd have completed this dissertation. I love you and I'm excited for what's next for us. Finally, I thank my parents, Subroto and Shanti, and my brother Aditya for their encouragement and support over the years.

1 Introduction

Vision is a rich modality for information to enter awareness, so much so that textbooks assert that "[m]ost of our impressions of the world and our memories of it are based on sight" (Kandel et al., 2021). It is no surprise, therefore, that the structure and function of the visual system have been studied intensively for centuries. By the end of the 19th century, much progress had been made. Decades of psychophysical experiments had measured perceptual phenomena in humans and derived laws linking properties of stimuli to the resulting percepts. James (1890) described then-current research into "the connection of conscious states with their physical conditions, including the whole of brain-physiology, and the recent minutely cultivated physiology of the sense-organs, together with [...] 'psycho-physics,' or the laws of correlation between sensations and the outward stimuli by which they are aroused".

Meanwhile, anatomical techniques had identified the projection from the retina to the lateral geniculate nucleus (LGN) and then to striate cortex as being critical to vision (Flechsig, 1896), and the retinotopic nature of this projection had been proposed (Willbrand, 1890). Later, Hubel and Wiesel (1962) suggested the idea of feed-forward hierarchical processing, in which the response properties of cells in visual cortex arose from their immediate LGN inputs. Since then, the subcortical and cortical components of the visual system have been extensively characterized in non-human primates and other animals via invasive anatomical techniques (Felleman and Van Essen, 1991).

While they provide great insight into the structure of the visual system, anatomical methods cannot produce data from awake, behaving humans. Non-invasive methods of recording brain data *in vivo* are necessary to resolve questions that rely on such data. In the late 20th and early 21st centuries, techniques such as functional magnetic resonance imaging (fMRI; Berns 1999) and magnetic resonance spectroscopy (MRS; Tognarelli et al., 2015) were developed for this purpose. These methods can provide unique insight into neural correlates of behavior in humans. Here, we present two studies that show the power of these non-invasive techniques for resolving questions of interest in neuroscience.

In Chapter 2, we use MRS to measure visual cortical γ−aminobutyric acid (GABA) concentrations in persons with amblyopia and normally-sighted persons. We then link these measurements with psychophysical measures of perceptual suppression in the same individuals. By combining these two modalities, we draw conclusions about the relationship between visual cortical GABA concentrations and visual perception in amblyopia and in normal human vision.

In Chapter 3, we use fMRI to identify many topographically-organized visual cortical areas as well as the two major subcortical driving inputs of visual cortex, the magnocellular and parvocellular pathways from retina to LGN to V1. We then simultaneously record from all of these identified areas while participants performed a task that differentially activated the two subcortical inputs. We analyze the coupling between the subcortical inputs and all identified visual cortical areas, and the effect of

spatial attention on this coupling. This study showcases a major advantage of fMRI, namely the ability to record from the entire brain simultaneously while engaging human behavioral faculties of interest.

1.1 References

Berns, G. S. (1999). Functional neuroimaging. *Life Sciences* 65, 2531–2540.

Felleman, D. J., and Van Essen, D. C. (1991). Distributed Hierarchical Processing in the Primate Cerebral Cortex. *Cerebral Cortex* 1, 1–47. doi: 10.1093/cercor/1.1.1.

Flechsig, P. E. (1896). *Gehirn und Seele*. Leipzig, Germany: Veit.

Hubel, D. H., and Wiesel, T. N. (1962). Receptive fields, binocular interaction and functional architecture in the cat's visual cortex. *J Physiol* 160, 106-154.2.

James, W. (1890). *The principles of psychology, Vol I.* New York, NY, US: Henry Holt and Co doi: 10.1037/10538-000.

Kandel, E. R., Koester, J. D., Mack, S. H., and Siegelbaum, S. A. (2021). "The Constructive Nature of Visual Processing," in *Principles of Neural Science, 6e* (New York, NY: McGraw Hill).

Tognarelli, J. M., Dawood, M., Shariff, M. I. F., Grover, V. P. B., Crossey, M. M. E., Cox, I. J., et al. (2015). Magnetic Resonance Spectroscopy: Principles and Techniques: Lessons for Clinicians. *J Clin Exp Hepatol* 5, 320–328. doi: 10.1016/j.jceh.2015.10.006.

Willbrand, H. (1890). *Die hemianopischen Gesichtsfeld-Formen und das optische Wahrnehmungszentrum*. Weisbaden, Germany: J. F. Bergmann.

2 Visual cortical GABA and perceptual suppression in amblyopia

This chapter, in full, is a republication of the material as it appears in Mukerji, A., Byrne, K. N., Yang, E., Levi, D. M., and Silver, M. A. (2022). Visual cortical γ−aminobutyric acid and perceptual suppression in amblyopia. *Frontiers in Human Neuroscience* 16. Available at: https://www.frontiersin.org/articles/10.3389/fnhum.2022.949395

2.1 Abstract

In amblyopia, abnormal visual experience during development leads to an enduring loss of visual acuity in adulthood. Physiological studies in animal models suggest that intracortical GABAergic inhibition may mediate visual deficits in amblyopia. To better understand the relationship between visual cortical γ-aminobutyric acid (GABA) and perceptual suppression in persons with amblyopia (PWA), we employed magnetic resonance spectroscopy (MRS) to quantify GABA levels in both PWA and normally-sighted persons (NSP). In the same individuals, we obtained psychophysical measures of perceptual suppression for a variety of ocular configurations. In PWA, we found a robust negative correlation between the depth of amblyopia (the difference in visual acuity between the amblyopic and non-amblyopic eyes) and GABA concentration that was specific to visual cortex and was not observed in a sensorimotor cortical control region. Moreover, lower levels of visual cortical GABA were associated with weaker perceptual suppression of the fellow eye by the amblyopic eye and stronger suppression of the amblyopic eye by the fellow eye. Taken together, our findings provide evidence that intracortical GABAergic inhibition is an important component of the pathology of human amblyopia and suggest possible therapeutic interventions to restore vision in the amblyopic eye through enhancement of visual cortical GABAergic signaling in PWA.

2.2 Introduction

Amblyopia is a neurodevelopmental disorder that results in deficits in multiple aspects of perception, including visual acuity, binocular vision, form vision, and motion perception (reviewed in Levi, 2013, 2020; Kiorpes, 2019). Amblyopia typically results from strabismus, anisometropia, cataract, ptosis, and/or other visual abnormalities (Webber and Wood, 2005). When these abnormalities occur during a critical period in early life, they interfere with the development of connections to and between visual cortical neurons. If amblyopia is not treated during this critical period, it can lead to perceptual deficits that persist even after correction of refractive error, ocular alignment, cataract, etc. (Fagiolini and Hensch, 2000; Levi et al., 2011; Birch, 2013). Amblyopia affects upto 3% of the world's population (Brown et al., 2000) and is therefore of significant clinical and neuroscientific interest.

There are substantial deficits in visual perception of stimuli presented to the amblyopic eye (Hamm et al., 2014) that have been extensively characterized using established psychophysical measures (McKee et al., 2003). In addition, persons with amblyopia (PWA) typically exhibit an imbalance in interocular perceptual suppression, in which the ability of inputs representing the amblyopic eye to suppress perception in the non-amblyopic ("fellow") eye is much weaker than suppression of perception in the amblyopic eye by stimuli presented to the fellow eye (e.g., Harrad and Hess, 1992). More recent work suggests that this asymmetry in interocular suppression contributes to many of the perceptual deficits associated with amblyopia (Li et al., 2011; Ding et al., 2013; Hess et al., 2014; Vedamurthy et al., 2015).

Physiological studies in animal models have shown that interocular suppression of visual responses occurs in early visual cortex (V1 and V2) and is correlated with the depth of amblyopia (Bi et al., 2011; Shooner et al., 2017). The primary inhibitory neurotransmitter in the brain is γ-aminobutyric acid (GABA), and visual cortical interocular suppression in animals with strabismus arises from inhibitory interactions that are mediated by GABA (Sengpiel et al., 2006). In addition, studies in human subjects with normal vision have related levels of visual cortical GABA and pharmacological manipulations of GABAergic signaling to perceptual measures of interocular suppression (Van Loon et al., 2013; Robertson et al., 2016; Mentch et al., 2019), and visual cortical GABA levels are rapidly altered by global changes in visual inputs (Lunghi et al., 2015; Kurcyus et al., 2018). GABAergic inhibition has also been linked to many aspects of visual function and development, including the onset and closure of the developmental critical period (Fagiolini et al., 2004; Sale et al., 2010).

Magnetic resonance spectroscopy (MRS) allows non-invasive measurements of GABA concentrations in awake, behaving humans (Near et al., 2013; Greenhouse et al., 2016), thereby facilitating investigation of GABA's contributions to perception (Yoon et al., 2010; Van Loon et al., 2013). Here, we employed MRS to measure visual cortical GABA concentrations in PWA and normally-sighted persons (NSP) and correlated these GABA levels with psychophysical measures of perceptual suppression, including interocular suppression. In particular, we focused on surround suppression, in which perception of a target stimulus is impaired by simultaneous presentation of a high-contrast stimulus that surrounds or is adjacent to the target (Chubb et al., 1989; Xing and Heeger, 2001).

Results from animal studies support the idea that feedback from extrastriate visual cortical areas V2 and V3 to V1 and GABAergic inhibition are critical components of the neural circuitry that generates surround suppression (Angelucci and Bressloff, 2006; Alitto and Dan, 2010; Nassi et al., 2013). This is supported by a study in humans showing that fMRI responses in cortical area V1 to a binocularly presented stimulus are suppressed by presentation of a binocular surround (Zenger-Landolt and Heeger, 2003). In the present study, we measured GABA concentration in visual cortex using MRS and investigated its relationship to the depth of amblyopia and to psychophysical measures of surround suppression in PWA and NSP.

Both interocular and intraocular surround suppression are well-studied in NSP (e.g., Petrov and McKee, 2006; Schallmo and Murray, 2016), but there is less research

investigating surround suppression in PWA. Previous work from our group has indicated increased monocular surround suppression in the amblyopic eye of PWA relative to their fellow eye and to NSP (Huh et al., 2014). Other studies have shown that presentation of a stimulus to the fellow eye results in profound perceptual suppression of a target presented to the amblyopic eye at non-overlapping retinal locations (Thompson et al., 2019), whereas presentation of a stimulus to the amblyopic eye results in weak or absent suppression of the fellow eye (Huang et al., 2012). Our study extends this work by measuring both interocular and intraocular surround suppression and correlating these psychophysical measures with visual cortical GABA concentrations in the same individuals with amblyopia.

2.3 Materials and Methods

This study consisted of both MRS and psychophysical measurements in the same individuals. Thirty-one participants completed at least one of the surround suppression psychophysical conditions. We also acquired MRS data from 15 NSP (20/20 corrected vision), 14 of whom participated in psychophysics experiments, and from 16 PWA, 8 of whom participated in psychophysics experiments. Of the 16 PWA, 12 had anisometropic amblyopia, and 4 had a mixture of anisometropia and strabismus. All participants (both NSP and PWA) were evaluated by optometry residents and students during recruitment. Visual acuity with and without correction was tested using the Bailey-Lovie LogMAR chart (Table 1), and diagnoses were confirmed, if applicable. Acuity was re-tested and confirmed immediately before the beginning of psychophysical data collection. Additional clinical details are provided in Table 1. MRS data for two subjects were discarded due to quality issues (one with severe head motion and one with inadequate visual correction), leaving MRS data for 14 PWA.

Table 1: Clinical Data of Persons with Amblyopia (PWA).

Bolded subjects took part in psychophysics experiments.

Subject	Age	Sex	Amb type	Amb eye	Acuity in DE (logMAR)	Acuity in NDE (logMAR)
A1	52	F	Aniso	OD	-0.097	0.418
A2	30	F	Aniso	OS	-0.184	0.398
A3	19	M	Aniso	OD	-0.085	0.538
A4	50	F	Aniso	OS	-0.164	0.398
A5*	24	F	Aniso	OS	-0.057	0.281
A6	61	F	Aniso	OS	-0.097	0.497
A7	39	F	Aniso	OS	-0.097	0.244
A8	44	F	Aniso	OS	-0.204	0.261
A9	46	M	Aniso	OD	-0.097	0.281
A10*	33	M	Aniso	OS	-0.097	0.358
A11	36	M	Aniso	OD	-0.204	0.117
A12	25	M	Aniso	OS	-0.202	0.244
M1	43	F	Mixed	OS	-0.077	0.756
M2	33	F	Mixed	OS	-0.085	1.176
M3	61	F	Mixed	OS	0.077	0.602
M4	25	M	Mixed	OS	0	0.224

OS = left eye, OD = right eye

* MRS data from these subjects were discarded due to quality issues (severe head motion, poor visual correction)

The PWA group was comprised of 10 female and six male participants with a mean age of 38.8 years (SD = 13.0). The NSP group was comprised of eight female and seven male participants with a mean age of 38.7 years (SD = 14.7). Subjects in the PWA group were refracted and corrected for distance vision, and all participants wore their best correction during testing.

Magnetic resonance spectroscopy

We recorded proton MRS data using a 32-channel RF head coil in a Siemens Trio 3-Tesla MR scanner located in the Henry H. Wheeler, Jr. Brain Imaging Center. Each recording session consisted of two T1-weighted anatomical scans (sagittal MP-RAGE, TR/TE/TI = 1,900/2.52/900 ms, flip angle = 9°, FoV 250 × 176, 1 mm3 voxel size, acceleration factor of two) and eight MEGA-PRESS scans [320 transients per scan − 160 Off and 160 On, TR/TE = 1,500/68 ms, edit pulse frequencies of 1.9 ppm (On-resonance) and 7.5 ppm (Off-resonance), edit pulse bandwidth of 45 Hz, delta frequency of −1.7 ppm relative to water (chosen for signal detection at 3.00 ppm), water suppression bandwidth of 50 Hz, TA = 8.4 min]. MEGA-PRESS scans were collected in pairs, switching between On- and Off-resonance editing pulses.

MRS data were acquired from a 3 × 3 × 3 cm occipital cortical voxel centered bilaterally on the calcarine sulcus and parallel to the parieto-occipital sulcus (Figure 1).

Another 3 × 3 × 3 cm voxel served as a control and was centered over the hand knob area of the precentral gyrus in the right hemisphere. This control sensorimotor voxel was parallel to the superior-posterior axis, with the medial border of the voxel abutting the longitudinal fissure. This sensorimotor cortical area is easily defined based on gross anatomical landmarks and has been used as a region of interest in multiple previous MRS studies (Evans et al., 2010; Stagg et al., 2011; Greenhouse et al., 2016). Participants were asked to maintain fixation on a central point either on a uniform gray background or a contrast-reversing checkerboard visual stimulus that was presented to one or both eyes. GABA MRS measurements were averaged across these visual stimulation conditions. This procedure was based on results from MRS studies at high magnetic field strength that found no significant changes to visual cortical GABA levels due to visual stimulation (Lin et al., 2012; Schaller et al., 2013).

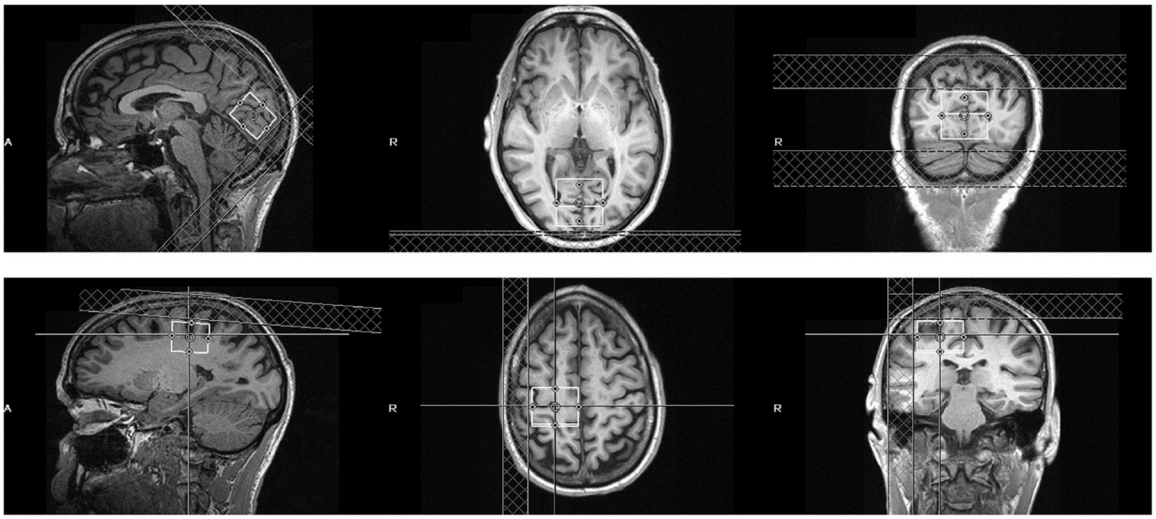

Figure 1. Position of the visual cortical MRS voxel (top row) and sensorimotor control voxel (bottom row) in an example subject. The voxel is 3 × 3 × 3 cm and centered bilaterally over the calcarine sulcus (visual cortex) or right precentral gyrus (sensorimotor control).

Spectroscopy data were analyzed according to the procedure described in Greenhouse et al. (2016). Sets of 10 consecutive transients were averaged and stored in a single Siemens rda file. This resulted in 32 rda files per scan (16 On and 16 Off). The data were preprocessed and analyzed with custom Matlab code implemented by Greenhouse et al. (2016). Analysis code can be downloaded at.1 Preprocessing included zero-padding from 1,024 to 4,096 data points and apodization with a 4-Hz Gaussian function. Off-resonance spectra were manually phase-corrected and aligned using creatine (Cr) as a reference. Correction values were applied to the paired On-resonance spectra (Evans et al., 2013; Near et al., 2014). Summary statistics were calculated for each frequency of each On- and Off-resonance spectrum, and the number of deviant values (>2 standard deviations from the mean) was tallied. The spectra were also visually inspected, and 7.7% of total spectra were excluded from further analysis, based on the number of deviant values and overt corruption or distortion of the spectra (Near et al., 2013; Simpson et al., 2017). Metabolite concentrations were estimated using peak integration methods that have been applied by others (Yoon et al., 2010; Greenhouse et

al., 2016; Maddock et al., 2016). GABA concentrations were calculated from the signal range of 2.85 and 3.15 ppm in the difference spectra, and creatine concentrations were calculated from the signal range of 2.93 and 3.10 ppm in the summed On- and Off-resonance spectra. GABA concentrations were then normalized by creatine by calculating the ratio of total GABA/total Creatine for each scan.

We found no significant difference between PWA and NSP in the proportion of gray matter in either the visual cortical or sensorimotor control MRS voxels [visual: $t(27) = 0.81$, $p = 0.42$; motor: $t(27) = 0.96$, $p = 0.34$]. Given this result, we did not perform additional normalization of the GABA:creatine ratio based on the proportion of gray matter.

Psychophysics

Apparatus

Stimuli were generated with MATLAB and the Psychophysics Toolbox (Brainard, 1997; Pelli, 1997) and were presented on the left and right halves of a gamma-corrected CRT monitor. We used a 1920 × 1440 screen resolution and a 75 Hz refresh rate. Stimuli were viewed centrally through a mirror stereoscope at a distance of 60 cm in a darkened room. Stimuli were always presented on a uniform gray background at mean luminance.

Stimuli and experimental procedures

Surround suppression is stronger for peripheral targets compared to foveal targets (Snowden and Hammett, 1998; Petrov et al., 2005; Lev and Polat, 2011). Thus, we chose to measure surround suppression in the near periphery with an annulus-shaped stimulus similar to those used in previous studies by our group as well as others (Zenger-Landolt and Heeger, 2003; Yoon et al., 2010; Kosovicheva et al., 2012). In addition, surround suppression is more pronounced for iso-oriented compared to cross-oriented surrounds (Xing and Heeger, 2001; Yoon et al., 2009). We therefore also measured the orientation selectivity of surround suppression and its relationship to visual cortical GABA.

The stimulus was a contrast reversing (4 Hz), sine-wave grating (1 cpd spatial frequency) presented within a circular aperture (Figure 2). Concentric black lines divided the stimulus into an annulus (in which the target was presented) and inner and outer surround regions. The annulus extended 3° to 4.5° (radii) of eccentricity from the center of the stimulus, and the outer surround region had a maximum eccentricity of 8° radius. The grating orientation within the annulus was always horizontal. In the iso-oriented condition, the inner and outer surround regions consisted of horizontal gratings that were phase aligned with the gratings in the annulus, and in the cross-surround condition, the gratings within the surround regions were vertically oriented. A black fixation point was present at the center of the image for both eyes at all times. Participants viewed the stimuli through a custom mirror stereoscope, and correct alignment of the two eyes' images was achieved by adjusting the mirrors so that vertical and horizontal Nonius lines could be seen by each eye and appeared as a cross. In addition, binocular fusion contours (seen by both eyes) encircling the stimuli were present at all times to promote stable binocular eye alignment.

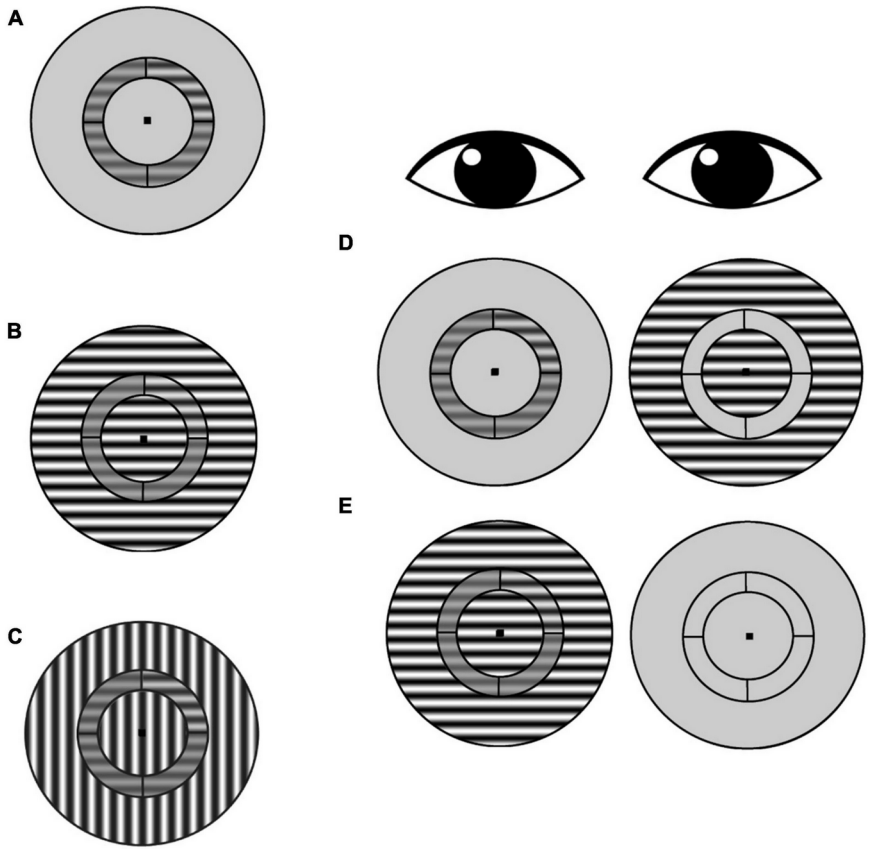

Figure 2. Surround suppression task. (A) Subjects were asked to identify which annulus quadrant contained a contrast increment relative to the pedestal contrast (in this example, the target contrast increment is in the upper right quadrant). This no-surround condition was used to estimate baseline contrast discrimination thresholds for each participant. (B) Iso-oriented condition: target-containing annulus and surround share the same orientation. (C) Cross-oriented condition: annulus and surround have orthogonal orientations. (D) Schematic of dichoptic presentation. The annulus was presented to one eye, and the surround was presented to the other eye. In this example, the surround is iso-oriented [as in (B)], but cross-oriented surrounds [as in (C)] were also tested. (E) Schematic of monocular presentation, with annulus and surround presented to one eye and only the fixation point presented to the other eye.

The annulus was divided by black lines into four quadrants of equal (30% Michelson) contrast. Participants were asked to indicate via keypress which quadrant contained the contrast increment (4-alternative forced choice). On each trial, the annulus and surround regions were simultaneously presented for 1 s to either the same eye (monocular trials) or to the two eyes separately (dichoptic trials). For baseline trials (no surround), the annulus was presented to one eye, while the other eye viewed the mean luminance background. The amount of contrast increment was determined for each trial using a 2-up, 1-down staircase procedure in steps of 0.125 log units. Each staircase terminated after 12 reversals, and contrast discrimination threshold for each staircase was defined as the average of the last six reversals. Participants had unlimited response time after stimuli were removed from the screen, and they were provided with auditory

feedback after every trial. Participants completed practice trials at the beginning of every session.

Surround regions were presented at 3–5 different Michelson contrast values that were individually determined for each participant. During the pilot phase of this study, we observed that some PWA failed to perceive even a maximum-contrast (99% Michelson) annulus with their amblyopic eye when the maximum-contrast surround was presented to the non-amblyopic eye. As a result, they were unable to detect any contrast increment within the annulus with their amblyopic eye. We therefore determined the maximum surround contrast at which thresholds could be estimated in all presentation conditions prior to the start of data collection for each participant. This contrast was then used as the maximum of the range of tested surround contrasts for a given participant, and the set of tested surround contrasts was identical across all experimental conditions for that participant.

Experimental design and statistical analysis

Presentation conditions

Participants were tested in eight different experimental conditions in a 2 (eye) × 2 (ocular configuration of center and surround stimuli; monocular or dichoptic) × 2 (relative surround orientation; cross- or iso-) factorial design plus a baseline (no surround) condition for each eye (Table 2). Trials in a given experimental condition were blocked, and within each block, staircases with different surround contrast values were randomly interleaved. For each participant, there were four staircases per experimental condition per surround contrast value. Data from additional staircases were collected when preliminary threshold estimates (computed as the average of the last six reversals) failed to converge.

Table 2: Schematic of surround suppression presentation conditions

DE: dominant eye (fellow eye for PWA)

NDE: non-dominant eye (amblyopic eye for PWA)

Condition	**Monocular DE**		**Monocular NDE**		**Dichoptic DE**		**Dichoptic NDE**	
Eye	Annulus	Surround	Annulus	Surround	Annulus	Surround	Annulus	Surround
DE			-	-		-	-	
NDE	-	-			-			-

For PWA, the amblyopic eye was the non-dominant eye (NDE), and the fellow eye was the dominant eye (DE). For NSP, the NDE was defined as the eye with the higher baseline (without a surround) contrast discrimination threshold, and the other eye was the DE. This definition is similar to others that have been used to measure sensory eye dominance (e.g., Wang et al., 2018), and it is more relevant to our study of perceptual measures than methods based on sighting dominance (Mapp et al., 2003).

In the monocular conditions, the annulus and surround were presented to the same eye (either monocular-DE or monocular-NDE) (Table 2). When the annulus and surround were shown to different eyes (dichoptic conditions), the conditions were labeled

according to which eye viewed the annulus. Thus, in the dichoptic-DE condition, the annulus was presented to the dominant eye and the surround to the non-dominant eye. The reverse ocular configuration was used in the dichoptic-NDE condition (Table 2). Taken together, these conditions allowed measurement of both directions of interocular surround suppression (DE suppressing NDE and NDE suppressing DE) as well as monocular surround suppression in both the DE and NDE.

Threshold estimation

For each condition and participant, we estimated the contrast increment needed to reliably identify the target quadrant (defined as the average of the contrast increment values of the last six reversals of each psychophysical staircase). Contrast discrimination thresholds were estimated for two baseline conditions in which a surround was absent (one for each eye) and for the eight conditions with a surround shown in Table 2, each tested with 3–5 different surround contrast values. These values ranged from 5 to 99% Michelson contrast (full data in Figure 3, top panel).

Psychophysical modeling

To correct for differences in baseline contrast discrimination thresholds across subjects and eyes, normalized values of both the estimated threshold and the presented surround contrast values were calculated by dividing by the subject's baseline (no surround) threshold for the eye which viewed the annulus, generating "relative threshold" and "relative surround contrast" values that were used for further analyses. As a result, a different set of relative surround contrast values were associated with each eye of each participant. However, to conduct group comparisons and correlations with visual cortical GABA levels, it is useful to obtain a single measure of contrast discrimination for each combination of eye, condition, and participant. We therefore initially attempted to fit the relative threshold vs. relative surround contrast function for each condition (Figure 3) with a model in order to derive a relative threshold level for specified relative surround contrast values, but there were often conditions that were not well fit by the model.

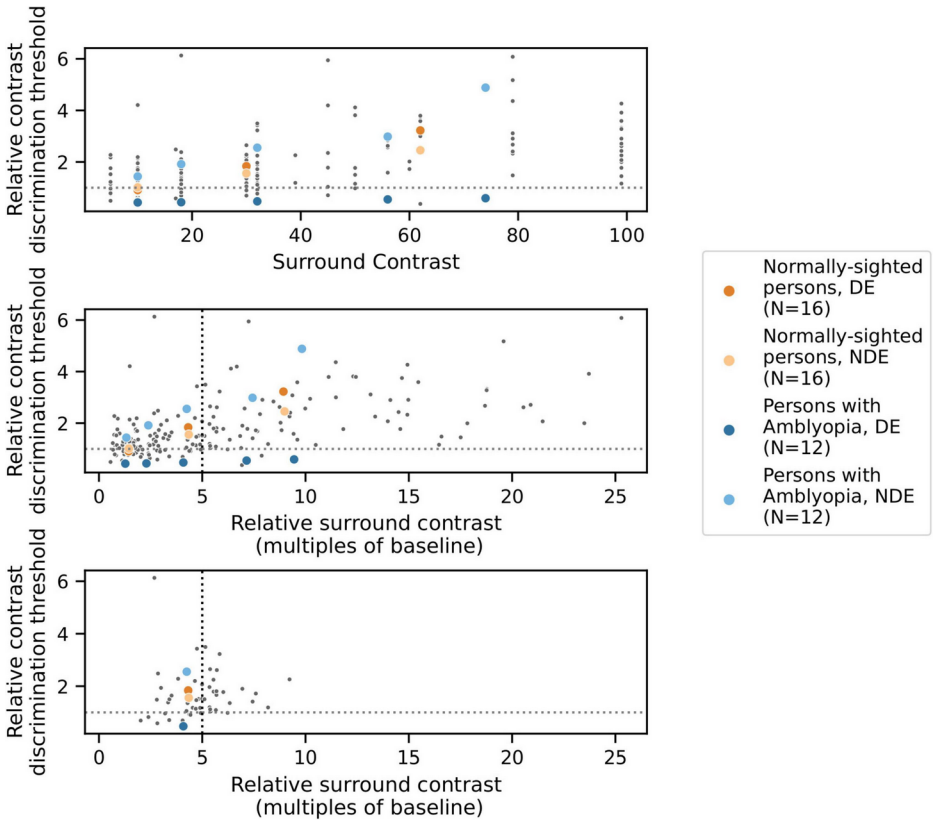

Figure 3. Results from one example condition (iso-oriented surround, dichoptic presentation) illustrating the psychophysical modeling approach. Data points indicate relative contrast discrimination thresholds for each eye when the surround was presented to the other eye. Observations from one PWA (blue) and one NSP (orange) are shown in color. Top: Normalized contrast discrimination threshold (y-axis) vs. unnormalized surround contrast (x-axis, expressed as Michelson contrast values). The y-axis indicates contrast discrimination thresholds that were normalized by the baseline (no surround) contrast discrimination threshold for each eye and each participant. As a result of the normalization, each subject's baseline values were rescaled to 1 for each eye and condition, and the horizontal line at y = 1 separates surround suppression (>1) from facilitation (<1). Middle: After normalization of surround contrasts. The x-axis represents the contrast of the surround as a multiple of the same baseline contrast discrimination threshold value used to normalize the contrast discrimination threshold values. The black vertical dotted line indicates the relative surround contrast value of five that we used to calculate a single relative contrast discrimination threshold value for each combination of eye, condition, and participant. Each of these thresholds was derived based on the relative surround contrast value that was closest to five. Bottom: The selected data points that were used for further analyses.

We therefore used a data-driven approach to obtain a single relative surround contrast level for the entire data set that was then used to compute a contrast discrimination threshold value for each combination of eye, condition, and participant. Specifically, we determined the relative surround contrast value across all of the data combined across all participants that satisfied the following constraints: (1) reliably evoked surround suppression (mean relative threshold > 1, indicating higher thresholds in

the presence of a surround), and (2) unbiased, in that analysis of data from one eye was not systematically based on higher relative surround contrasts compared to data from the other eye. Note that meeting the second criterion requires normalization by each eye's baseline contrast threshold, since the two eyes of PWA differ in absolute contrast sensitivity. In our data set, these constraints were best satisfied by a relative surround contrast value of approximately five (i.e., five times the baseline contrast discrimination threshold). For further analysis of each combination of eye, condition, and participant, we used the relative contrast discrimination threshold value from the data point that was closest to a relative surround contrast value of five (Figure 3). We also conducted our analyses over a range of relative surround contrast values from 2 to 10, and all results that are reported as statistically significant in this paper were robust across this range.

Statistics and tests

For all correlation analyses, we employed the Spearman's correlation coefficient (ρ) as a non-parametric measure of the strength of the relationship. Unlike the Pearson's correlation coefficient r, Spearman's ρ is calculated on ranks and therefore can reveal both linear and non-linear correlations. Like Pearson's r, it ranges from -1 (indicating perfect negative correlation) to + 1 (perfect positive correlation).

In addition, we used permutation testing to generate 100,000-element distributions of ρ values under the null hypothesis, thereby avoiding assumptions about the shapes of the distributions of the recorded data. For each statistical test involving correlations, we rejected the null hypothesis if the observed ρ was more extreme than 95% of the values in the null distribution, corresponding to a two-tailed test with $\alpha = 0.05$.

To characterize the relationships between visual cortical GABA and perceptual surround suppression, we first tested whether the Spearman's correlation coefficient ρ was significantly different from 0 for each eye and ocular configuration, indicating evidence for an association between GABA and the magnitude of surround suppression for that eye and ocular configuration. Secondly, we compared ρ values between the two eyes for the two complementary dichoptic presentations, allowing us to test for possible interocular differences in the relationship between GABA and surround suppression. Analogous tests were conducted for the monocular conditions. Finally, we compared the amplitude of interocular differences in surround suppression between PWA and NSP to test for differences between groups.

2.4 Results

Our main finding was that the correlations between visual cortical GABA and interocular perceptual suppression are different for the two eyes of PWA. This difference was due to a more positive correlation of visual cortical GABA with suppression of the dominant eye (DE) and a more negative correlation of GABA with suppression of the non-dominant eye (NDE). This pattern was observed for both cross-oriented surrounds (Figure 4) and iso-oriented surrounds (Figure 5). For cross-oriented surrounds, this difference between the DE and NDE was significant for both monocular ($p = 0.04$) and

dichoptic (p = 0.048) presentation conditions. For iso-oriented surrounds, this difference was significant for dichoptic presentation (p = 0.036).

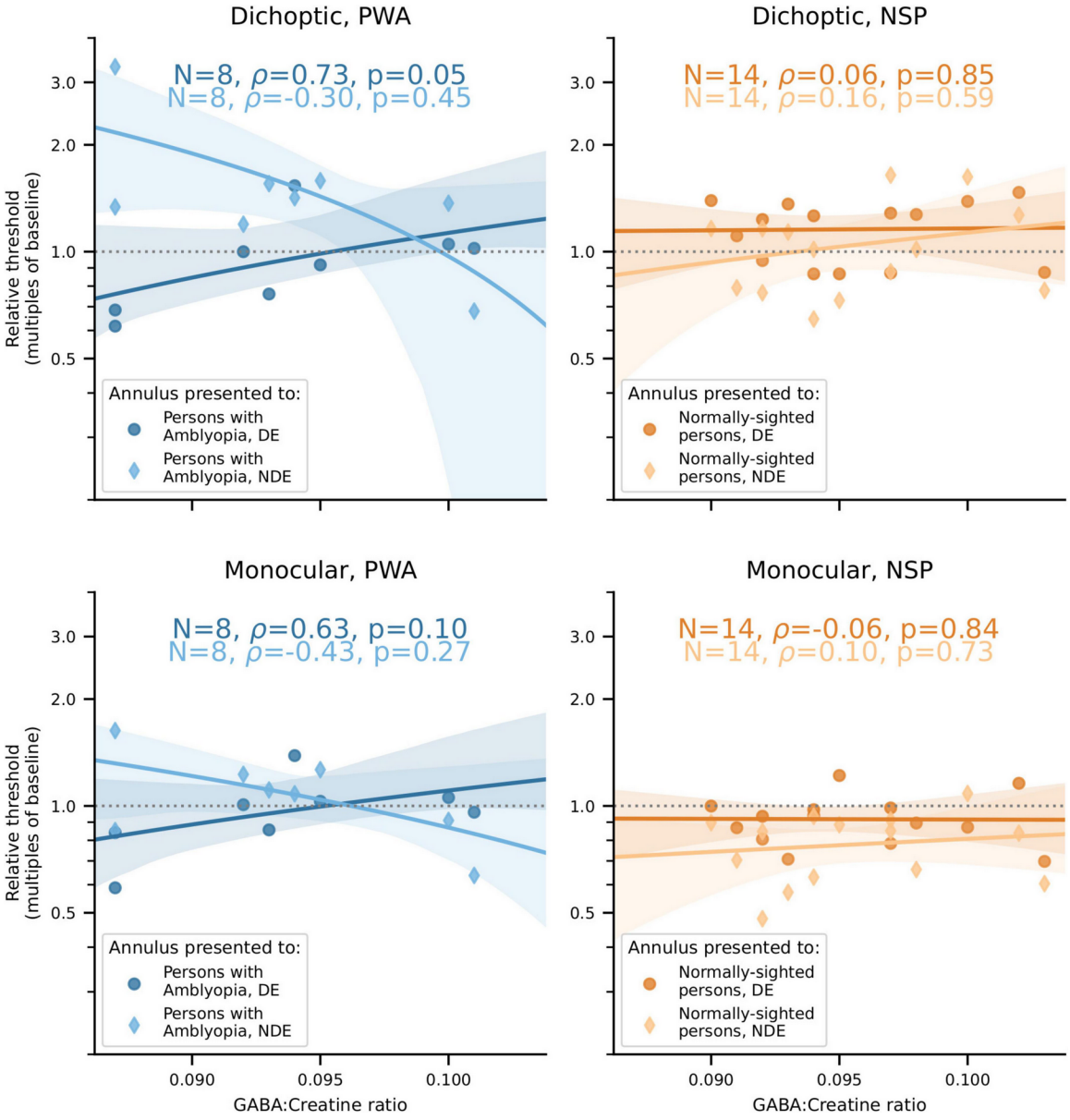

Figure 4. Relationships between cross-oriented surround suppression (Figure 2C) and visual cortical GABA levels. Top row: Dichoptic presentation. Bottom row: Monocular presentation. Left column: PWA. Right column: NSP. Shading indicates 95% bootstrapped confidence intervals of the best linear fit. The difference in the strength of the GABA/surround suppression correlation between the two eyes of PWA was significant for monocular (p = 0.04) and dichoptic (p = 0.048) presentation.

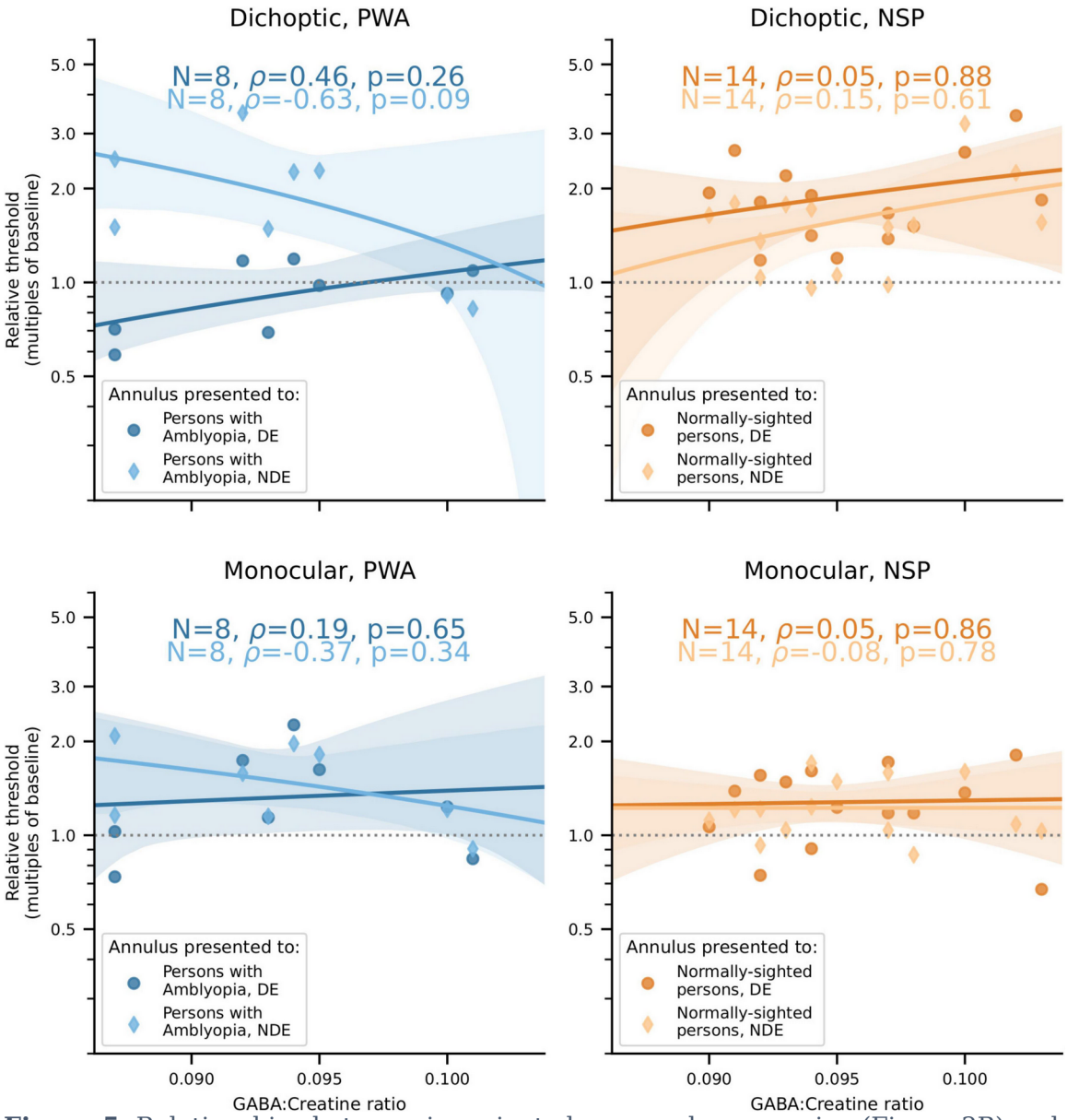

Figure 5. Relationships between iso-oriented surround suppression (Figure 2B) and visual cortical GABA levels. Top row: Dichoptic presentation. Bottom row: Monocular presentation. Left column: PWA. Right column: NSP. Shading indicates 95% bootstrapped confidence intervals of the best linear fit. The difference in the strength of the GABA/surround suppression correlation between the two eyes of PWA was significant for dichoptic presentation ($p = 0.036$).

When these analyses were carried out using GABA concentrations from the sensorimotor control voxel, none of these correlations or differences were significant (all $p > 0.18$ except one $p = 0.10$). Additionally, we tested for anatomical specificity by comparing the difference of correlation coefficient values obtained from the visual cortical and from the sensorimotor control MRS voxels to the permutation distribution of these difference values generated by the bootstrap procedure. While these tests were not significant for any measure (all $p > 0.07$), several approached significance with $p < 0.10$. The consistent and significant results observed with visual cortical (but not sensorimotor)

GABA concentrations provides some support for the finding that correlations between visual cortical GABA and interocular perceptual suppression are different for the two eyes of PWA.

In the following sections we show how we arrived at these conclusions, beginning with presentation of MRS results, then psychophysical results, and finally correlations between these brain and behavioral measures.

No significant difference between persons with amblyopia and normally-sighted persons in visual cortical γ-aminobutyric acid levels

We first compared visual cortical GABA levels for PWA and NSP by using the ratio of GABA to creatine within the MRS voxel for each subject (Figure 6). We did not find a significant difference in visual cortical GABA levels between PWA and NSP [two-tailed t-test; $t(27) = -0.75$; $p = 0.46$].

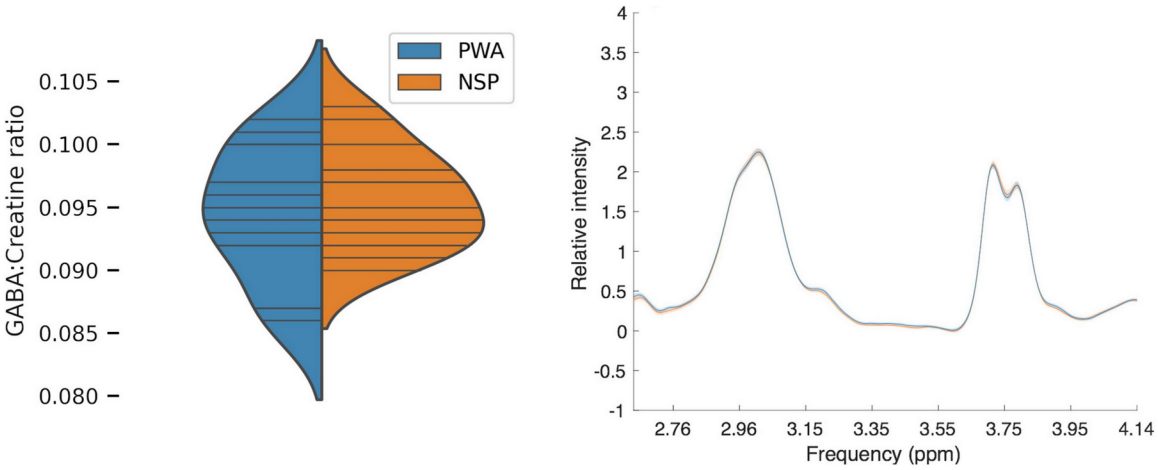

Figure 6. Left: Plot of MRS GABA:creatine ratio values in visual cortex. Blue, persons with amblyopia (N = 14; mean = 0.09, SEM = 0.001). Orange, normally sighted persons (N = 15; mean = 0.09, SEM = 0.001). Horizontal lines indicate visual cortical GABA levels in individual participants, and plotted distributions are kernel density estimates. There was no significant difference in visual cortical GABA levels between the two groups. Right: Mean normalized MRS spectra for PWA (blue) and NSP (orange). Width of colored regions indicates standard error of the mean. The mean normalized spectra are very similar for the two groups.

Depth of amblyopia is significantly inversely correlated with visual cortical γ-aminobutyric acid in persons with amblyopia

Importantly, we found a significant negative relationship ($\rho = -0.61$, $p = 0.02$, $N = 14$) between visual cortical GABA concentration and depth of amblyopia, as measured by interocular difference in visual acuity (Figure 7). That is, lower levels of GABA were associated with more severe amblyopia. A control MRS voxel located in sensorimotor cortex showed no significant relationship ($\rho = 0.10$, $p = 0.78$, $N = 11$). The difference in Fisher-transformed correlation values between GABA MRS levels in the two cortical locations corresponds to a z-score of 1.74 and a two-tailed p-value of 0.08. This result, combined with our findings of different correlations between perceptual suppression and visual cortical GABA for the DE and NDE in PWA (Figures 4, 5), provide further

evidence of a relationship between abnormal interocular interactions and reduced GABAergic visual cortical inhibition in amblyopia.

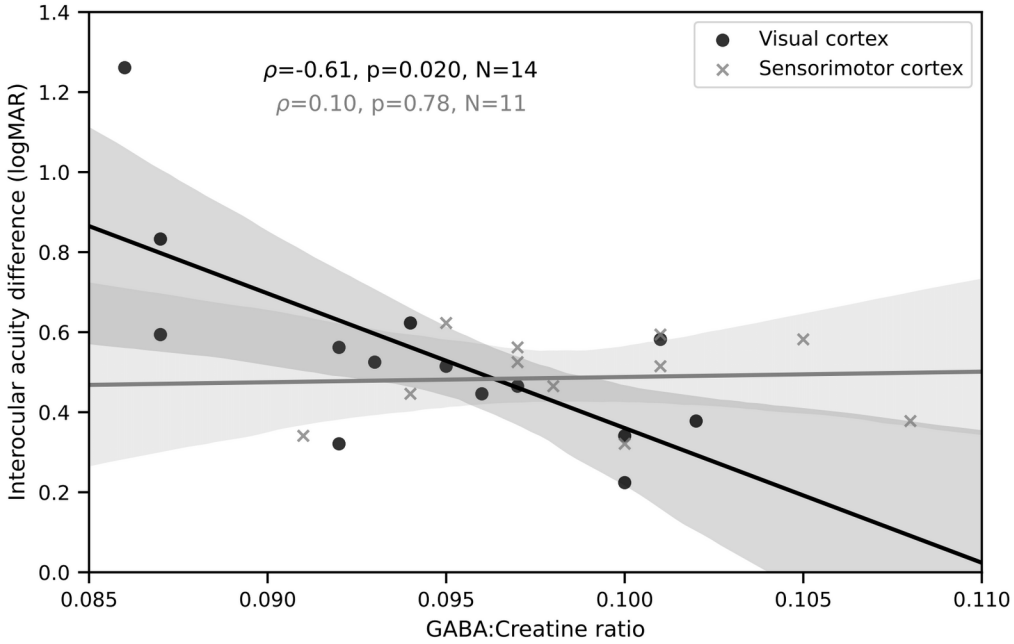

Figure 7. Visual cortical GABA levels predict differences in visual acuity between the two eyes in persons with amblyopia. Shaded regions are bootstrapped 95% confidence intervals of the best linear fit.

Interocular differences in contrast discrimination in persons with amblyopia

Baseline (i.e., in the absence of a surround) contrast discrimination thresholds are plotted in Figure 8. As expected from the literature on perceptual deficits in amblyopia (e.g., Levi, 2013), contrast discrimination thresholds were lower in the fellow (dominant, DE) eye of PWA compared to the amblyopic (non-dominant, NDE) eye [two-tailed t-test; $t(11) = 2.68$; $p = 0.02$]. The NSP group did not have a clinically designated dominant eye, so the eye with the lower baseline contrast discrimination threshold was defined as the DE and the eye with the higher threshold as the NDE for participants in this group. We do not present results from inferential statistical testing of interocular differences in contrast discrimination threshold values for NSP, as the classification of the DE and NDE was based on these threshold values for this group. The effect size was smaller for PWA (0.77) than for NSP (1.21).

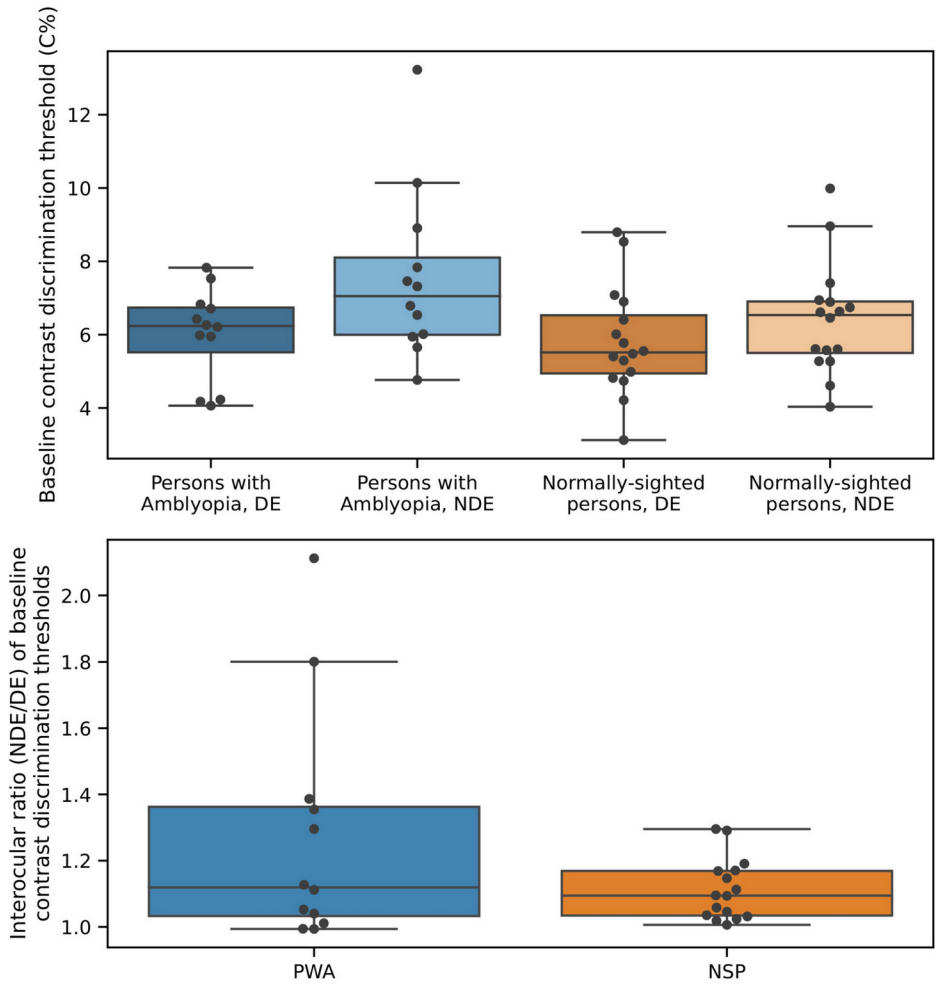

Figure 8. Baseline contrast discrimination thresholds differ between the two eyes of persons with amblyopia. Top: Baseline contrast discrimination thresholds. Bottom: Interocular difference in baseline contrast discrimination thresholds.

Interocular perceptual suppression of the non-dominant eye by the dominant eye is significantly greater than that of the dominant eye by the non-dominant eye in persons with amblyopia

An omnibus ANOVA (Table 3) of the surround suppression data showed significant main effects of surround orientation (cross- or iso-oriented surround), ocular configuration (dichoptic or monocular), and eye (DE or NDE). The main effect of group (PWA or NSP) was not significant. In addition, three significant interactions were observed: Ocular Configuration × Eye, Group × Eye, and Ocular Configuration × Group × Eye.

Table 3: Omnibus ANOVA results

Effect	F	p (>F)
Orientation	34.41	1.74×10^{-8}*
Ocular Configuration	19.55	1.58×10^{-5}*
Eye	6.94	0.009*
Group	2.26	0.134
Ocular Configuration x Eye	4.80	0.030*
Group x Eye	24.87	1.29×10^{-6}*
Ocular Configuration x Group x Eye	9.46	2.38×10^{-3}*

When the annulus and surround were presented to different eyes (dichoptic presentation) in PWA, we found significantly more interocular perceptual suppression of the NDE by the DE compared to the amount of suppression of the DE by the NDE (Figure 9). In particular, we used two-tailed one-sample t-tests to evaluate whether the ratio of suppression for annuli presented to the NDE vs. to the DE was different from a value of 1. This ratio was unequal and highly significant for both cross-oriented and iso-oriented surrounds in PWA. No such significant differences were observed for NSP for dichoptic presentation. Note that none of these differences in PWA are due to interocular differences in contrast discrimination, as surround suppression values were calculated from data that were normalized by contrast discrimination threshold values obtained from the baseline (no surround) condition for each eye of each participant (Figure 3).

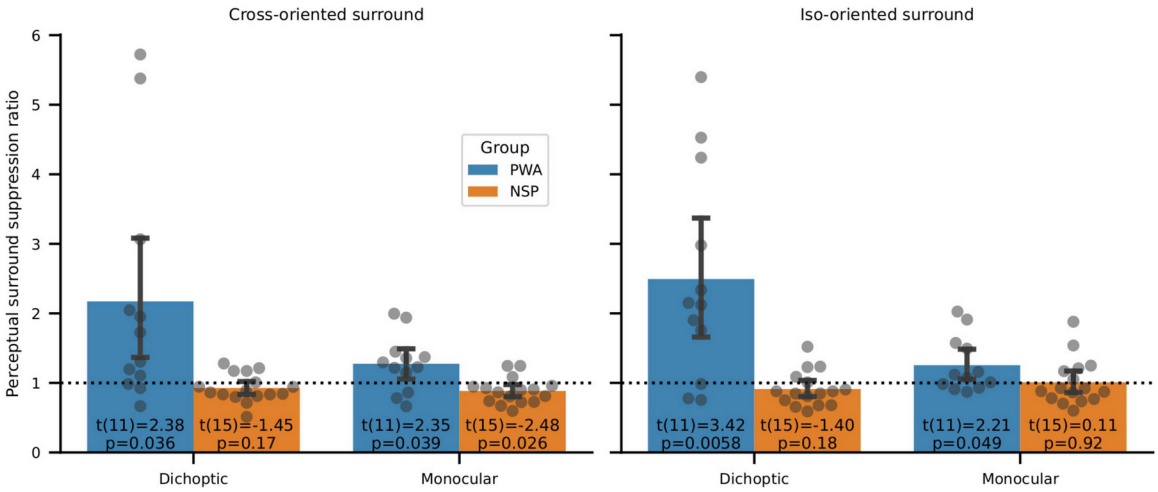

Figure 9. Perceptual surround suppression. Data points are NDE:DE suppression ratios for individual subjects. Bars indicate means and standard errors. In PWA, one-sample t-tests of whether suppression ratios were different from a value of 1 showed significantly more suppression of the DE than the NDE in all four conditions (cross- and iso-oriented surrounds and dichoptic and monocular conditions). Suppression ratios were not significantly different from a value of 1 for NSP in 3 out of 4 conditions, and the fourth condition (cross-oriented surround, monocular presentation) showed a significant difference in the opposite direction from PWA (i.e., more suppression in the NDE than the DE).

When the annulus and surround were presented to the same eye (monocular condition), we observed greater suppression in the NDE than the DE in PWA (Figure 9). This difference was significant for both cross-oriented and iso-oriented surrounds. We observed the opposite pattern in the NSP group (more suppression in the DE than the NDE), and this difference was significant for monocular presentation.

For PWA, stereo vision was assessed with the Randot Circles test during clinical assessment. Stereoacuity was not significantly correlated with interocular perceptual suppression ratio for any of the four conditions (cross- and iso-oriented surrounds, dichoptic and monocular conditions; all $|\rho| < 0.44$, all $p > 0.15$) or with the depth of amblyopia ($\rho = 0.26$, $p > 0.37$). Additionally, depth of amblyopia was not significant correlated with interocular perceptual suppression ratio for any of the four conditions (all $|\rho| < 0.27$, all $p > 0.53$).

Replication of previous reports of psychophysical orientation-selective surround suppression

Surround suppression has previously been shown to be orientation-selective, with iso-oriented surrounds producing stronger perceptual suppression than cross-oriented surrounds (Xing and Heeger, 2001; Yoon et al., 2009). We tested whether these previous findings of perceptual orientation-selective surround suppression (OSSS) were replicated in our data set. We calculated the orientation selectivity of surround suppression for each participant by computing the ratio of the relative contrast discrimination threshold values in the iso- and cross-oriented surround conditions. We then used two-tailed one-sample t-tests to evaluate whether these interocular OSSS ratios were different from a value of 1. We found strong evidence of orientation-selective surround suppression for six out of eight configurations that we tested (Figure 10). This result is in agreement with prior literature on orientation-selective surround suppression (Xing and Heeger, 2001; Yoon et al., 2009). The only conditions in which highly significant OSSS was not observed were in PWA with dichoptic presentation, where interocular differences due to amblyopia may have overwhelmed detection of OSSS.

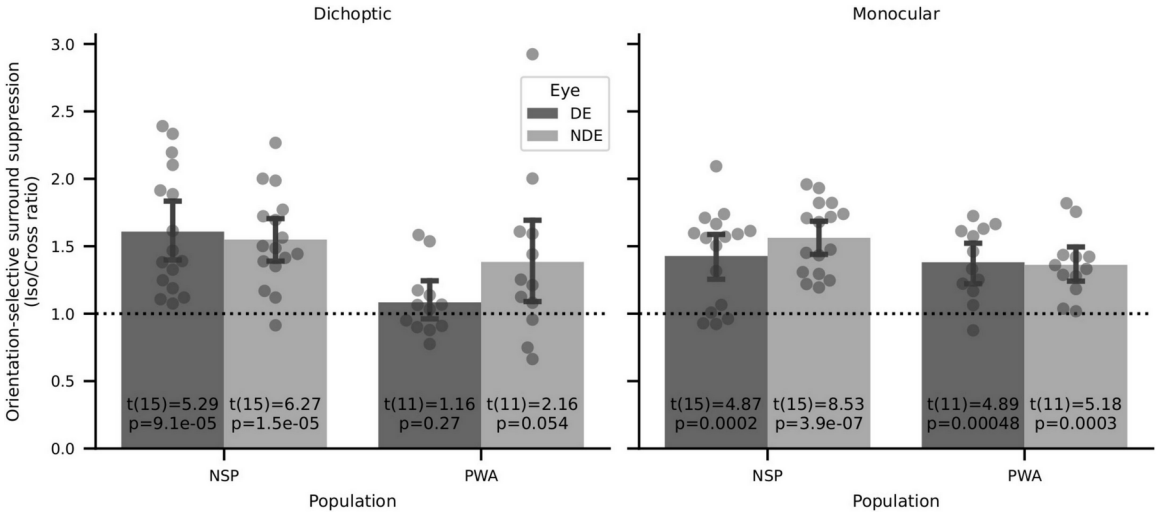

Figure 10. Orientation-selective surround suppression (OSSS) results. Two-sided one-sample t-tests of iso/cross suppression ratios showed significant OSSS in 6 of 8 conditions, including all four for normally sighted persons.

No significant correlation between visual cortical γ-aminobutyric acid and the strength of orientation-selective surround suppression

We also analyzed the relationship between visual cortical GABA and orientation-selective surround suppression (the ratio of relative contrast discrimination threshold values for iso- and cross-oriented configurations). We found strong orientation-selective surround suppression when considering all participants who took part in the psychophysics experiments (Figure 10), and this was also evident in the subset of subjects who had both MRS and psychophysical data (14 NSP and 8 PWA). However, in contrast to the results reported in Yoon et al. (2010), we observed no significant correlations between the strength of this orientation-selective surround suppression and visual cortical GABA levels (all $|\rho| < 0.5$, all $p > 0.2$).

No significant relationship between visual cortical γ-aminobutyric acid and contrast discrimination in either persons with amblyopia or normally-sighted persons

We found no significant relationship between visual cortical GABA levels and baseline (no-surround) contrast discrimination in either PWA or NSP (Figure 11).

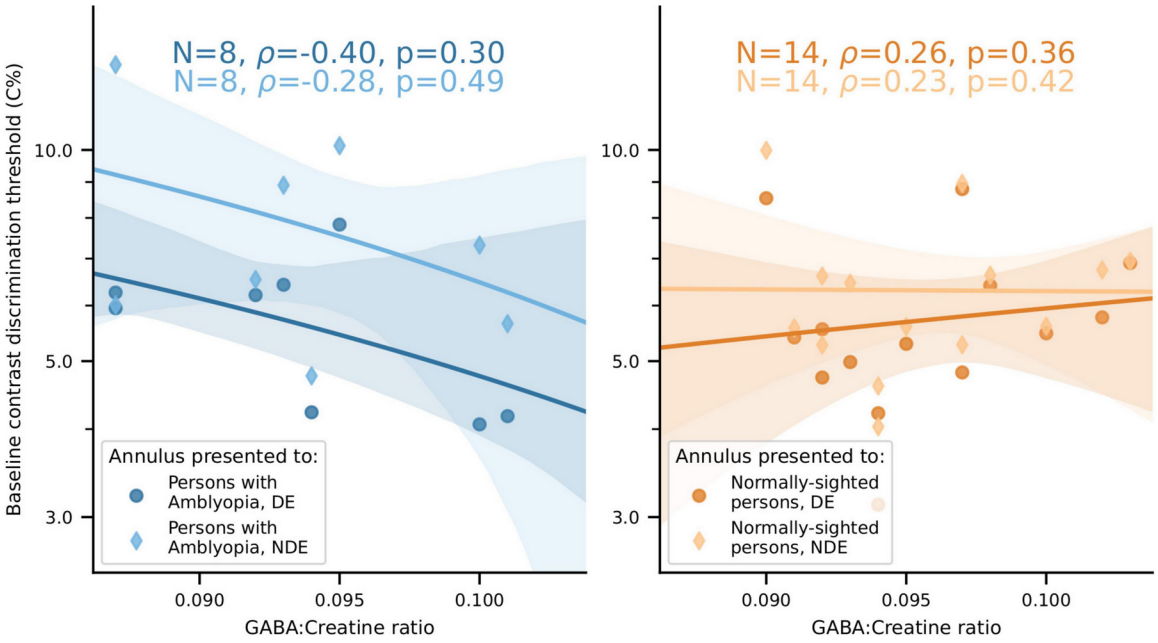

Figure 11. No significant relationship between visual cortical GABA levels and baseline contrast discrimination thresholds for either PWA or NSP. Left, PWA. Right, NSP. Marker shape and color indicate the eye that viewed the annulus. Shaded regions are bootstrapped 95% confidence intervals of the best linear fit.

2.5 Discussion

We found that, on average, PWA do not have significantly different levels of visual cortical GABA compared to NSP. However, we observed a significant negative correlation between visual cortical GABA concentration and depth of amblyopia in this group, as measured by interocular difference in visual acuity. We also found significant

differences between the two eyes in PWA in the strength of the correlation between visual cortical GABA and interocular suppression: for both cross- and iso-oriented surrounds, individuals with less GABA generally had weaker suppression of the fellow eye by the amblyopic eye and stronger suppression of the amblyopic eye by the fellow eye.

Isolating perceptual suppression by controlling for baseline contrast discrimination performance

Our surround suppression task required subjects to determine which quadrant in the annulus had a higher contrast than the other three quadrants, and the contrast difference between the quadrants at threshold quantified task performance. These contrast discrimination thresholds are influenced by both the modulatory effects of the surround and intrinsic contrast discrimination ability. This represents a potential confound for the study of perceptual suppression, particularly given that PWA exhibit many perceptual deficits when viewing with their amblyopic eye (Levi, 2020).

To control for differences in contrast discrimination across participants and eyes, we measured contrast discrimination thresholds in the absence of a surround. We found a significant difference in these baseline contrast thresholds between the fellow and amblyopic eyes in PWA, as expected (Figure 8). We then quantified surround suppression by expressing contrast discrimination thresholds in the presence of a surround as multiples of the baseline threshold for that participant and eye (Figure 3). This effectively controlled for variations in intrinsic contrast discrimination ability across participants and eyes and enabled us to assess task performance with a metric that isolates the effects of the surround on contrast discrimination.

Orientation selectivity of perceptual surround suppression

Our surround suppression task measures the effects of a high contrast surround on contrast discrimination of a center (annulus) stimulus in both monocular and dichoptic configurations. We replicated previous studies (Xing and Heeger, 2001; Yoon et al., 2009; Kosovicheva et al., 2012) showing that the magnitude of surround suppression depends on the relative orientation of the center and surround stimuli, with iso-oriented stimuli producing the strongest surround suppression (Figure 10).

Visual cortical γ-aminobutyric acid, interocular suppression, and surround suppression

Research in animal models has suggested that intracortical GABAergic inhibition is a major contributor to surround suppression (Adesnik et al., 2012; Nassi et al., 2013), but there is also evidence for other mechanisms, including a reduction in subcortical excitatory inputs (Ozeki et al., 2004; Ozeki et al., 2009). Studies in humans have also been mixed, with some supporting intracortical GABAergic inhibition in surround suppression (Zenger-Landolt and Heeger, 2003) and others favoring withdrawal of excitation (Schallmo et al., 2018). In addition, recent studies have suggested that there are distinct neural mechanisms underlying intraocular and interocular surround suppression (Schallmo and Murray, 2016). In the present study, both intraocular (monocular) and interocular (dichoptic) stimulus configurations revealed differences between the DE and NDE in the relationship between visual cortical GABA and surround suppression in PWA.

GABAergic inhibition has also been implicated in interocular suppression of neuronal and perceptual responses. In these studies, stimuli are presented to corresponding retinal locations in the two eyes, unlike surround suppression, in which the annulus and surround were presented to adjacent but non-overlapping retinal locations, either monocularly or dichoptically. Local administration of the GABAA receptor antagonist bicuculline strongly reduced interocular suppression of sensory responses in primary visual cortical neurons in strabismic cats (Sengpiel et al., 2006). Perceptual suppression in binocular rivalry in NSP is correlated with visual cortical GABA levels, as measured with MRS (Robertson et al., 2016), and is modulated by pharmacological alterations of GABAergic signaling (Mentch et al., 2019). Moreover, GABA visual cortical levels and administration of the GABAA receptor agonist lorazepam are both associated with fewer perceptual switches and longer mean perceptual duration in binocular rivalry in NSP (Van Loon et al., 2013). These results, together with evidence that intracortical GABAergic inhibition contributes to surround suppression, helped to motivate the present study by suggesting that visual cortical GABA levels might be a biomarker for aspects of interocular perceptual suppression in PWA.

Interocular perceptual suppression in amblyopia

Multiple psychophysical studies have shown a positive correlation between interocular perceptual suppression and the depth of amblyopia (Li et al., 2011; Vedamurthy et al., 2015; reviewed in Hess et al., 2014). One apparent exception is the study by Holopigian et al. (1988), which reported a negative correlation between the magnitude of interocular suppression and the depth of amblyopia. However, Holopigian et al. (1988) only studied suppression of the amblyopic eye by the fellow eye, using a small (1.2°) stimulus.

Physiologically, interocular suppression of responses in cortical area V2 is highly correlated with depth of amblyopia in strabismic macaque monkeys (Bi et al., 2011). Studies in PWA that have accounted for differences in monocular thresholds in the two eyes have found that suppression of the amblyopic eye by the fellow eye is similar to that observed in individuals with normal vision, but suppression of the fellow eye by the amblyopic eye is abnormally weak (Huang et al., 2012; Ding et al., 2013; Ding and Levi, 2014; Zhou et al., 2018; Gong et al., 2020). This pattern of asymmetric contrast gain (Ding et al., 2013; Ding and Levi, 2014) was also observed in responses to dichoptic masking stimuli in cortical areas V1 and V2 of amblyopic macaque monkeys, in which suppression of amblyopic eye responses by presentation of a mask to the fellow eye was normal, while the amblyopic eye was ineffective in suppressing responses to visual stimuli presented to the fellow eye (Shooner et al., 2017).

These studies are consistent with the idea that at least some visual deficits in amblyopia are due to insufficient suppression of fellow eye responses by inputs from the amblyopic eye. Our results support this notion by relating both the depth of amblyopia as well as the differences between the DE and NDE in surround suppression to visual cortical GABA levels in PWA.

Given the relationships between visual cortical GABA and perceptual and clinical measures of interocular interactions in amblyopia that we observed, it is perhaps surprising that there was no significant difference between PWA and NSP in overall

visual cortical GABA levels in our study. It may be that correlations of GABA levels with a continuous variable (like perceptual suppression or depth of amblyopia) may be more sensitive than a categorical comparison of GABA levels in PWA and NSP. It is also possible that the abnormal visual experience that causes amblyopia alters the relationship between visual cortical GABA concentrations and perceptual outcomes, perhaps because of a compensatory process that results in the characteristic perceptual deficits observed in amblyopia.

Limitations

Challenges in recruiting PWA that met the clinical criteria and the large number of psychophysical and MRS sessions that were required for our study imposed limits on the sample sizes for measuring correlations between visual cortical GABA levels and perceptual measures in PWA. Replicating some of the results that we report here in a larger sample with greater statistical power is an important future direction. However, evidence from three separate GABA/behavior correlations supports a relationship between reduced GABAergic visual cortical inhibition and abnormal interocular interactions in amblyopia. First, lower levels of GABA were significantly correlated with greater severity of amblyopia, as measured by interocular acuity difference. Also, less visual cortical GABA was associated with relatively weaker perceptual suppression of the fellow eye by the amblyopic eye and relatively stronger suppression of the amblyopic eye by the fellow eye. The two eyes significantly differed from each other in the correlations between visual cortical GABA and interocular suppression for both cross-oriented and iso-oriented surrounds in PWA. Even though we did not perform corrections for multiple comparisons, these converging results from three distinct perceptual data sets provide strong evidence for an important role of intracortical GABAergic inhibition in balancing interocular interactions in PWA and suggest that visual cortical GABA levels could be a biomarker for amblyopia.

Visual cortical GABAergic inhibition as a potential therapeutic target in amblyopia

Our results support a framework in which people with severe amblyopia have reduced visual cortical GABA levels that are associated with abnormally weak suppression of the fellow eye by the amblyopic eye. Pharmacological enhancement of GABAergic signaling in visual cortex could therefore be a possible treatment for the symptoms of amblyopia in adults.

Pharmacological elevation of GABAergic inhibition could also be combined with other therapeutic interventions that influence visual cortical activity. There is substantial evidence of rapid activity-dependent regulation of visual cortical GABA in the adult visual system. Short-term (2.5 h) monocular deprivation in NSP reduces visual cortical GABA, as measured with MRS (Lunghi et al., 2015). Also, opening the eyes in darkness decreases GABA levels in visual cortex of NSP, and visual cortical GABA levels during visual processing predict performance on a visual orientation discrimination task (Kurcyus et al., 2018). In addition, several weeks of monocular deprivation in adult macaque monkeys reduces histochemical markers for GABA and glutamic acid decarboxylase (the enzyme that synthesizes GABA) specifically in deprived-eye ocular dominance columns in primary visual cortex (Hendry and Jones, 1986). Interventions that enhance GABAergic signaling could be coupled with existing behavioral training procedures that use dichoptic tasks to improve visual function in the amblyopic eye (Hess

et al., 2010; Li et al., 2013; Vedamurthy et al., 2015). We note that most of these procedures have been aimed at perceptually "balancing" input from the two eyes. However, our results indicate that an alternative approach may be to train the amblyopic eye to suppress the fellow eye more effectively.

Conclusion

In summary, we found a negative correlation between the depth of amblyopia (interocular difference in visual acuity) and GABA concentration that was specific to visual cortex and was not observed in a sensorimotor cortical control region. In addition, the two eyes of PWA differed in their relationships between dichoptic interocular suppression and visual cortical GABA levels, for both cross- and iso-oriented surrounds: visual cortical GABA levels tended to be more positively correlated with perceptual suppression of the fellow eye by the amblyopic eye and more negatively correlated with suppression of the amblyopic eye by the fellow eye. These findings indicate that therapeutic interventions to enhance the ability of the amblyopic eye to suppress the fellow eye through intracortical GABAergic inhibition may be a promising avenue of future research in the treatment of adult amblyopia.

2.6 Data Availability Statement

The datasets presented in this study can be found in online repositories. The names of the repository/repositories and accession number(s) can be found below: https://github.com/smerdis/mukerji_etal_2022.

2.7 Ethics Statement

The studies involving human participants were reviewed and approved by the Committee for the Protection of Human Subjects at the University of California, Berkeley. The patients/participants provided their written informed consent to participate in this study.

2.8 Author Contributions

EY, DL, and MS designed the study. EY and KB collected the data. AM, KB, and EY analyzed the data. All authors contributed in writing the manuscript.

2.9 Funding

This work was supported by the National Eye Institute at the National Institutes of Health (R01 EY020976 to DL, T32 EY007043 to EY, and P30 EY003176) and the National Science Foundation Major Research Instrumentation Program (BCS-0821855).

2.10 Acknowledgments

We thank Betina Ip and Holly Bridge for their helpful comments on an earlier draft of the manuscript.

2.11 Conflict of Interest Statement

The authors declare that the research was conducted in the absence of any commercial or financial relationships that could be construed as a potential conflict of interest.

2.12 References

Adesnik, H., Bruns, W., Taniguchi, H., Huang, Z. J., and Scanziani, M. (2012). A neural circuit for spatial summation in visual cortex. Nature 490, 226–231. doi: 10.1038/nature11526.

Alitto, H. J., and Dan, Y. (2010). Function of inhibition in visual cortical processing. Current Opinion in Neurobiology 20, 340–346. doi: 10.1016/j.conb.2010.02.012.

Angelucci, A., and Bressloff, P. C. (2006). "Contribution of feedforward, lateral and feedback connections to the classical receptive field center and extra-classical receptive field surround of primate V1 neurons," in Progress in Brain Research Visual Perception., eds. S. Martinez-Conde, S. L. Macknik, L. M. Martinez, J.-M. Alonso, and P. U. Tse (Elsevier), 93–120. doi: 10.1016/S0079-6123(06)54005-1.

Baker, D. H., Meese, T. S., and Hess, R. F. (2008). Contrast masking in strabismic amblyopia: Attenuation, noise, interocular suppression and binocular summation. Vision Research 48, 1625–1640. doi: 10.1016/j.visres.2008.04.017.

Bi, H., Zhang, B., Tao, X., Harwerth, R. S., Smith, E. L., and Chino, Y. M. (2011). Neuronal Responses in Visual Area V2 (V2) of Macaque Monkeys with Strabismic Amblyopia. Cerebral Cortex 21, 2033–2045. doi: 10.1093/cercor/bhq272.

Birch, E. E. (2013). Amblyopia and Binocular Vision. Prog Retin Eye Res 33, 67–84. doi: 10.1016/j.preteyeres.2012.11.001.

Brainard, D. H. (1997). The Psychophysics Toolbox. Spatial Vision 10, 433–436. doi: 10.1163/156856897X00357.

Brown, S. A., Weih, L. M., Fu, C. L., Dimitrov, P., Taylor, H. R., and McCarty, C. A. (2000). Prevalence of amblyopia and associated refractive errors in an adult population in Victoria, Australia. Ophthalmic Epidemiol 7, 249–258.

Chubb, C., Sperling, G., and Solomon, J. A. (1989). Texture interactions determine perceived contrast. PNAS 86, 9631–9635. doi: 10.1073/pnas.86.23.9631.

Ding, J., Klein, S. A., and Levi, D. M. (2013). Binocular combination in abnormal binocular vision. Journal of Vision 13, 14. doi: 10.1167/13.2.14.

Docker for Mac release notes (2021). Docker Documentation. Available at: https://docs.docker.com/docker-for-mac/release-notes/ [Accessed July 21, 2021].

Evans, C. J., McGonigle, D. J., and Edden, R. A. E. (2010). Diurnal stability of gamma-aminobutyric acid concentration in visual and sensorimotor cortex. J Magn Reson Imaging 31, 204–209. doi: 10.1002/jmri.21996.

Evans, C. J., Puts, N. A. J., Robson, S. E., Boy, F., McGonigle, D. J., Sumner, P., et al. (2013). Subtraction artifacts and frequency (Mis-)alignment in J-difference GABA editing. Journal of Magnetic Resonance Imaging 38, 970–975. doi: 10.1002/jmri.23923.

Fagiolini, M., Fritschy, J.-M., Löw, K., Möhler, H., Rudolph, U., and Hensch, T. K. (2004). Specific GABAA Circuits for Visual Cortical Plasticity. Science 303, 1681–1683. doi: 10.1126/science.1091032.

Fagiolini, M., and Hensch, T. K. (2000). Inhibitory threshold for critical-period activation in primary visual cortex. Nature 404, 183–186. doi: 10.1038/35004582.

Greenhouse, I., Noah, S., Maddock, R. J., and Ivry, R. B. (2016). Individual differences in GABA content are reliable but are not uniform across the human cortex. NeuroImage 139, 1–7. doi: 10.1016/j.neuroimage.2016.06.007.

Hallum, L. E., Shooner, C., Kumbhani, R. D., Kelly, J. G., García-Marín, V., Majaj, N. J., et al. (2017). Altered Balance of Receptive Field Excitation and Suppression in Visual Cortex of Amblyopic Macaque Monkeys. The Journal of Neuroscience 37, 8216–8226. doi: 10.1523/JNEUROSCI.0449-17.2017.

Hamm, L. M., Black, J., Dai, S., and Thompson, B. (2014). Global processing in amblyopia: a review. Front. Psychol. 5. doi: 10.3389/fpsyg.2014.00583.

Harrad, R. (1996). Psychophysics of suppression. Eye 10, 270–273. doi: 10.1038/eye.1996.57.

Hensch, T. K., Fagiolini, M., Mataga, N., Stryker, M. P., Baekkeskov, S., and Kash, S. F. (1998). Local GABA circuit control of experience-dependent plasticity in developing visual cortex. Science 282, 1504–1508. doi: 10.1126/science.282.5393.1504.

Hess, R. F., Thompson, B., and Baker, D. H. (2014). Binocular vision in amblyopia: structure, suppression and plasticity. Ophthalmic and Physiological Optics 34, 146–162. doi: 10.1111/opo.12123.

Holopigian, K., Blake, R., and Greenwaldf, M. J. (1988). Clinical Suppression and Amblyopia. Investigative Ophthalmology & Visual Science 29, 444–451.

Huang, Z. J., Kirkwood, A., Pizzorusso, T., Porciatti, V., Morales, B., Bear, M. F., et al. (1999). BDNF regulates the maturation of inhibition and the critical period of plasticity in mouse visual cortex. Cell 98, 739–755. doi: 10.1016/s0092-8674(00)81509-3.

Kolasinski, J., Logan, J. P., Hinson, E. L., Manners, D., Divanbeighi Zand, A. P., Makin, T. R., et al. (2017). A Mechanistic Link from GABA to Cortical Architecture and Perception. Current Biology 27, 1685-1691.e3. doi: 10.1016/j.cub.2017.04.055.

Levi, D. M. (2013). Linking assumptions in amblyopia. Visual Neuroscience 30, 277–287. doi: 10.1017/S0952523813000023.

Levi, D. M. Rethinking amblyopia 2020. 12.

Levi, D. M., McKee, S. P., and Movshon, J. A. (2011). Visual deficits in anisometropia. Vision Res. 51, 48–57. doi: 10.1016/j.visres.2010.09.029.

Li, J., Thompson, B., Lam, C. S. Y., Deng, D., Chan, L. Y. L., Maehara, G., et al. (2011). The Role of Suppression in Amblyopia. Invest. Ophthalmol. Vis. Sci. 52, 4169–4176. doi: 10.1167/iovs.11-7233.

Lin, Y., Stephenson, M. C., Xin, L., Napolitano, A., and Morris, P. G. (2012). Investigating the Metabolic Changes due to Visual Stimulation using Functional Proton Magnetic Resonance Spectroscopy at 7 T. J Cereb Blood Flow Metab 32, 1484–1495. doi: 10.1038/jcbfm.2012.33.

Lunghi, C., Emir, U. E., Morrone, M. C., and Bridge, H. (2015). Short-Term Monocular Deprivation Alters GABA in the Adult Human Visual Cortex. Current Biology 25, 1496–1501. doi: 10.1016/j.cub.2015.04.021.

Maddock, R. J., Casazza, G. A., Fernandez, D. H., and Maddock, M. I. (2016). Acute Modulation of Cortical Glutamate and GABA Content by Physical Activity. J Neurosci 36, 2449–2457. doi: 10.1523/JNEUROSCI.3455-15.2016.

Mapp, A. P., Ono, H., and Barbeito, R. (2003). What does the dominant eye dominate? A brief and somewhat contentious review. Perception & Psychophysics 65, 310–317. doi: 10.3758/BF03194802.

McKee, S. P., Levi, D. M., and Movshon, J. A. (2003). The pattern of visual deficits in amblyopia. Journal of Vision 3, 5. doi: 10.1167/3.5.5.

Meese, T. S., Georgeson, M. A., and Baker, D. H. (2006). Binocular contrast vision at and above threshold. Journal of Vision 6, 7–7. doi: 10.1167/6.11.7.

Mentch, J., Spiegel, A., Ricciardi, C., and Robertson, C. E. (2019). GABAergic Inhibition Gates Perceptual Awareness During Binocular Rivalry. J. Neurosci. 39, 8398–8407. doi: 10.1523/JNEUROSCI.0836-19.2019.

Nassi, J. J., Lomber, S. G., and Born, R. T. (2013). Corticocortical Feedback Contributes to Surround Suppression in V1 of the Alert Primate. Journal of Neuroscience 33, 8504–8517. doi: 10.1523/JNEUROSCI.5124-12.2013.

Near, J., Andersson, J., Maron, E., Mekle, R., Gruetter, R., Cowen, P., et al. (2013). Unedited in vivo detection and quantification of γ-aminobutyric acid in the occipital cortex using short-TE MRS at 3 T. NMR Biomed 26, 1353–1362. doi: 10.1002/nbm.2960.

Near, J., Ho, Y.-C. L., Sandberg, K., Kumaragamage, C., and Blicher, J. U. (2014). Long-term reproducibility of GABA magnetic resonance spectroscopy. Neuroimage 99, 191–196. doi: 10.1016/j.neuroimage.2014.05.059.

Ozeki, H., Finn, I. M., Schaffer, E. S., Miller, K. D., and Ferster, D. (2009). Inhibitory Stabilization of the Cortical Network Underlies Visual Surround Suppression. Neuron 62, 578–592. doi: 10.1016/j.neuron.2009.03.028.

Ozeki, H., Sadakane, O., Akasaki, T., Naito, T., Shimegi, S., and Sato, H. (2004). Relationship between Excitation and Inhibition Underlying Size Tuning and Contextual Response Modulation in the Cat Primary Visual Cortex. J Neurosci 24, 1428–1438. doi: 10.1523/JNEUROSCI.3852-03.2004.

Pelli, D. G. (1997). The VideoToolbox software for visual psychophysics: transforming numbers into movies. Spatial Vision 10, 437–442. doi: 10.1163/156856897X00366.

Petrov, Y., Carandini, M., and McKee, S. (2005). Two Distinct Mechanisms of Suppression in Human Vision. J. Neurosci. 25, 8704–8707. doi: 10.1523/JNEUROSCI.2871-05.2005.

Pitchaimuthu, K., Wu, Q., Carter, O., Nguyen, B. N., Ahn, S., Egan, G. F., et al. (2017). Occipital GABA levels in older adults and their relationship to visual perceptual suppression. Scientific Reports 7. doi: 10.1038/s41598-017-14577-5.

Relationship between physiological measures of excitability and levels of glutamate and GABA in the human motor cortex - Stagg - 2011 - The Journal of Physiology - Wiley Online Library Available at: https://physoc.onlinelibrary.wiley.com/doi/10.1113/jphysiol.2011.216978 [Accessed June 28, 2021].

Sale, A., Berardi, N., Spolidoro, M., Baroncelli, L., and Maffei, L. (2010). GABAergic Inhibition in Visual Cortical Plasticity. Front Cell Neurosci 4. doi: 10.3389/fncel.2010.00010.

Schaller, B., Mekle, R., Xin, L., Kunz, N., and Gruetter, R. (2013). Net increase of lactate and glutamate concentration in activated human visual cortex detected with magnetic resonance spectroscopy at 7 tesla. Journal of Neuroscience Research 91, 1076–1083. doi: 10.1002/jnr.23194.

Schallmo, M.-P., Kale, A. M., Millin, R., Flevaris, A. V., Brkanac, Z., Edden, R. A., et al. (2018). Suppression and facilitation of human neural responses. eLife. doi: 10.7554/eLife.30334.

Schallmo, M.-P., and Murray, S. O. (2016). Identifying separate components of surround suppression. Journal of Vision 16, 2. doi: 10.1167/16.1.2.

Sengpiel, F., Jirmann, K.-U., Vorobyov, V., and Eysel, U. T. (2006). Strabismic suppression is mediated by inhibitory interactions in the primary visual cortex. Cereb. Cortex 16, 1750–1758. doi: 10.1093/cercor/bhj110.

Shooner, C., Hallum, L. E., Kumbhani, R. D., García-Marín, V., Kelly, J. G., Majaj, N. J., et al. (2017). Asymmetric Dichoptic Masking in Visual Cortex of Amblyopic Macaque Monkeys. The Journal of Neuroscience 37, 8734–8741. doi: 10.1523/JNEUROSCI.1760-17.2017.

Shooner, C., Hallum, L. E., Kumbhani, R. D., Ziemba, C. M., Garcia-Marin, V., Kelly, J. G., et al. (2015). Population representation of visual information in areas V1 and V2 of amblyopic macaques. Vision Research 114, 56–67. doi: 10.1016/j.visres.2015.01.012.

Simpson, R., Devenyi, G. A., Jezzard, P., Hennessy, T. J., and Near, J. (2017). Advanced processing and simulation of MRS data using the FID appliance (FID-A)—An open source, MATLAB-based toolkit. Magnetic Resonance in Medicine 77, 23–33. doi: 10.1002/mrm.26091.

Snowden, R. J., and Hammett, S. T. (1998). The effects of surround contrast on contrast thresholds, perceived contrast and contrast discrimination. Vision Research 38, 1935–1945. doi: 10.1016/S0042-6989(97)00379-9.

Song, C., Sandberg, K., Andersen, L. M., Blicher, J. U., and Rees, G. (2017). Human Occipital and Parietal GABA Selectively Influence Visual Perception of Orientation and Size. The Journal of Neuroscience 37, 8929–8937. doi: 10.1523/JNEUROSCI.3945-16.2017.

Stagg, C. J., Bestmann, S., Constantinescu, A. O., Moreno, L. M., Allman, C., Mekle, R., et al. (2011). Relationship between physiological measures of excitability and levels of glutamate and GABA in the human motor cortex. The Journal of Physiology 589, 5845–5855. doi: 10.1113/jphysiol.2011.216978.

Thompson, B., Maehara, G., Goddard, E., Farivar, R., Mansouri, B., and Hess, R. F. (2019). Long-Range Interocular Suppression in Adults with Strabismic Amblyopia: A Pilot fMRI Study. Vision (Basel) 3. doi: 10.3390/vision3010002.

Vedamurthy, I., Nahum, M., Bavelier, D., and Levi, D. M. (2015). Mechanisms of recovery of visual function in adult amblyopia through a tailored action video game. Scientific Reports 5. doi: 10.1038/srep08482.

Wang, Y., Cui, L., He, Z., Lin, W., Qu, J., Lu, F., et al. (2018). On the Relationship Between Sensory Eye Dominance and Stereopsis in the Normal-Sighted Adult Population: Normative Data. Frontiers in Human Neuroscience 12, 357. doi: 10.3389/fnhum.2018.00357.

Webber, A. L., and Wood, J. (2005). Amblyopia: prevalence, natural history, functional effects and treatment. Clin Exp Optom 88, 365–375. doi: 10.1111/j.1444-0938.2005.tb05102.x.

Xing, J., and Heeger, D. J. (2001). Measurement and modeling of center-surround suppression and enhancement. Vision Research 41, 571–583. doi: 10.1016/S0042-6989(00)00270-4.

Yoon, J. H., Maddock, R. J., Rokem, A., Silver, M. A., Minzenberg, M. J., Ragland, J. D., et al. (2010). GABA Concentration Is Reduced in Visual Cortex in Schizophrenia and Correlates with Orientation-Specific Surround Suppression. J. Neurosci. 30, 3777–3781. doi: 10.1523/JNEUROSCI.6158-09.2010.

Zenger-Landolt, B., and Heeger, D. J. (2003). Response Suppression in V1 Agrees with Psychophysics of Surround Masking. The Journal of Neuroscience 23, 6884–6893. doi: 10.1523/JNEUROSCI.23-17-06884.2003.

3 Functional coupling of lateral geniculate nucleus subdivisions with topographically-organized cortical areas

3.1 Introduction

The primary driving input of visual cortical neurons is the disynaptic projection from the retina to the lateral geniculate nucleus (LGN) of the thalamus and thence to primary visual cortex (V1; Jones, 1985; Sherman and Guillery, 2001). Within this pathway, distinct populations of retinal ganglion cells (RGCs) project to either magnocellular or parvocellular layers of the primate LGN. The six major layers of the primate LGN are labeled magnocellular (M, layers 1 and 2) and parvocellular (P, layers 2-6) based on the size of the neurons therein and the pattern of retinal inputs they receive. M and P LGN neurons also respond differently to visual stimulation (Wiesel and Hubel, 1966). M neurons exhibit high contrast sensitivity and transient responses to stimuli, whereas P neurons exhibit low contrast sensitivity and sustained responses to stimuli. Additionally, M neurons have low spatial resolution and are not responsive to color, while P neurons have high spatial resolution and are responsive to color (Hubel and Livingstone, 1990). Each layer of the left and right LGN receives topographically-organized input from one eye, thereby maintaining a retinotopic map of the contralateral visual hemifield (Kastner, Schneider, and Wunderlich, 2006).

The afferent projection from LGN to visual cortex also preserves topographic organization and thus creates a map of the contralateral visual hemifield in V1. This was the first cortical retinotopic map to be identified and is the earliest in the cortical visual processing hierarchy (see Wandell, Dumoulin and Brewer, 2007 for a review). The M and P layers of the LGN both project to input layer IV of V1, constituting parallel disynaptic input streams from retina to visual cortex via the LGN (hereafter referred to as the M and P subcortical inputs).

Subsequently, functional magnetic resonance imaging (fMRI) and population receptive field (pRF) mapping have been used to identify many other retinotopic maps in human visual cortex (Dumoulin and Wandell, 2008). Functional MRI allows for noninvasive recording of neural activity in awake behaving humans, and pRF analysis reveals the locations in the visual field that maximally excite a given voxel (volumetric pixel). Numerous human cortical visual areas can be defined on the basis of these pRF maps (Dumoulin and Wandell, 2008; Amano et al., 2009).

Separately, primate studies have identified dozens of cortical visual areas in macaques and arranged them into a hierarchy based on the pattern of anatomical projections between areas (Felleman and Van Essen, 1991). Many early visual areas are conserved across humans and macaques, such as V1, V2, and V3, but beyond these, the relationships and possible homologies between human and macaque cortical areas becomes more unclear (Orban, Van Essen, and Vanduffel, 2004).

In both non-human primates and humans, the pattern of connections among the areas of the cortical visual hierarchy suggests the existence of two processing streams with minimal cross-talk (Mishkin and Ungerleider, 1982; Ungerleider and Haxby, 1994). These are typically referred to as the dorsal and ventral streams and are specialized for different aspects of vision. The dorsal stream has been shown to be involved in spatial vision (Goodale et al, 1994) and motion processing (Braddick et al., 2001). In contrast, the ventral stream is critical for a variety of object recognition tasks involving shape and color (Gaffan, Harrison, and Gaffan, 1986) as well as face processing (Grill-Spector et al., 2017). The names "what" and "where" pathways have been used for the ventral and dorsal streams, respectively, due to this functional specialization.

The dorsal stream processes motion and requires high temporal resolution information supplied by the magnocellular input, while the ventral stream performs object and face recognition that depends on high spatial resolution information from the parvocellular input. It has therefore been suggested (Livingstone and Hubel, 1984) that the dorsal and ventral streams are extensions of the subcortical M and P inputs, respectively. However, it is now accepted that the ventral stream receives major inputs from both the M and P pathways, while the dorsal stream is mostly, but not totally, reliant on the M input (Merigan and Maunsell, 1993).

We employed fMRI to quantify and measure functional coupling between each of the M and P subdivisions of the LGN and topographically-organized dorsal and ventral stream cortical areas in awake behaving humans. This technique allows simultaneous noninvasive recordings from all of these areas. We used a previously described technique to localize the M and P subregions of the LGN in individual subjects using fMRI at 3 T field strength (Denison et al., 2014). Interregional functional coupling in fMRI data was quantified using timeseries coherence, a measure that is robust to differences in the shape of the hemodynamic response function across brain areas (Sun et al., 2004).

Spatial attention has been shown to enhance fMRI responses in the LGN (O'Connor et al., 2002; Schneider and Kastner, 2009), early visual cortical areas (Gandhi, Heeger, and Boynton, 1999; Silver, Ress, and Heeger, 2007), and in topographically-organized areas in the intraparietal sulcus (IPS; Silver, Rees, and Heeger, 2005). Spatial attention has also been shown to affect coupling between parietal and occipital cortex (Bressler et al., 2008; Lauritzen et al., 2009). We therefore sought to quantify the effect of spatial attention on coupling between the LGN and cortical visual areas.

In this study, we identified the M and P LGN subdivisions and many topographically-organized visual cortical areas in each participant. We then measured the strength of functional coupling between them under visual stimulation designed to preferentially drive either the magno- or parvocellular streams. We also measured the effect of spatial attention on the strength of functional coupling.

3.2 Materials and Methods

This study consisted of three functional MRI components: localization of M and P subdivisions of the LGN, cortical pRF mapping, and functional coupling. The same subjects took part in all components of the experiment (Table 1).

Subjects

Five adult subjects (25-30 years of age; 1 male, 4 female) participated in the study. All subjects provided written informed consent, and all experimental protocols were approved by the Committee for the Protection of Human Subjects at the University of California, Berkeley. Subjects had normal or corrected-to-normal visual acuity.

Table 1

Subject	M/P LGN localizer (min)*	pRF mapping (min)*	M/P coupling (min)*
S1	45	240	100
S2	40	240	105
S3	45	240	120
S4	50	240	120
S5	50	240	120

* indicates minutes of fMRI data acquisition for each component

Visual Display

MATLAB (The MathWorks Inc., Natick, MA) and Psychophysics Toolbox (Brainard, 1997; Pelli, 1997) were used to generate visual stimuli for the M/P LGN localizer and coupling tasks. Python and PsychoPy (Peirce et al., 2019) were used to generate stimuli for the pRF mapping task. All stimuli were displayed using gamma-corrected projection systems. An Avotec SV-6011 (Avotec, Inc., Stuart, FL) liquid crystal display projector was used to project stimuli onto a translucent screen located in the scanner bore behind the subject's head. A mirror was mounted over the subject's eyes to provide a view of the screen with a viewing distance of 32 cm.

Visual Stimuli

LGN localization

This portion of the study used the stimuli described in Denison et al. (2014). The LGN was initially localized using an alternating hemifield stimulus (Fig. 1A). A 100% contrast checkerboard pattern that reversed contrast polarity at 4 Hz covered either the left or right half of the screen. The other half of the screen contained a neutral grey background of . For the duration of the run, a white fixation point subtending 0.2° of visual angle was presented at the center of the screen. Subjects were instructed to maintain fixation while viewing the stimuli. The checkerboard alternated between the left and right halves of the screen every 13.5 seconds. A total of 11 left-right cycles were presented, corresponding to 297 seconds of visual stimulation. Two hemifield localizer runs were collected per subject for a total of about 10 minutes of scan time.

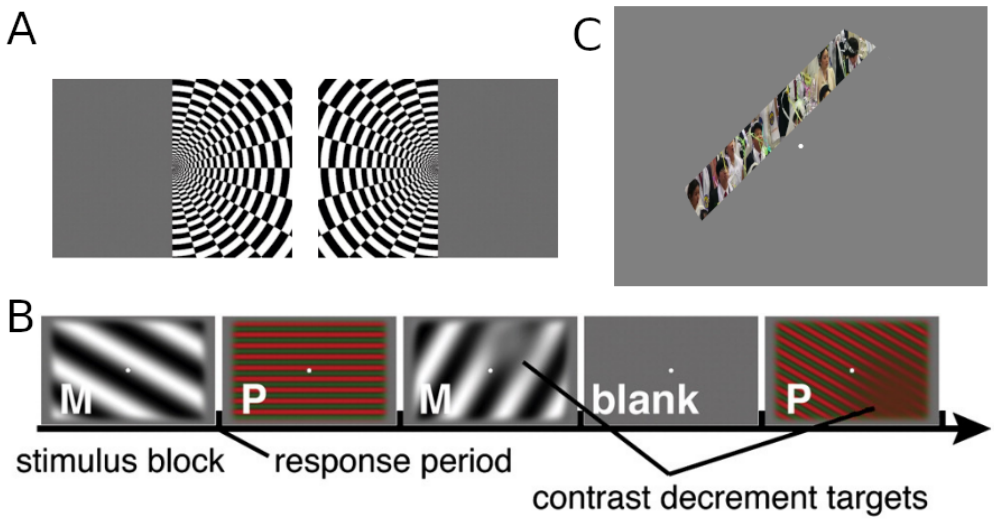

Figure 1. Task Stimuli. A) Hemifield localizer. B) M/P localizer C) Cortical pRF mapping. Adapted from Denison et al., 2014.

The M/P localizer stimulus from Denison et al., 2014 (Fig. 1B) was designed to differentially activate voxels with greater M- versus P-type responses. This localizer consisted of 18-second blocks of "M stimuli", "P stimuli", and blank (fixation point only) stimuli. The M and P stimuli both consisted of full-field sinusoidal gratings with sinusoidal counterphase flicker. To avoid sharp visual edges, the outer borders of the stimulus faded into the grey background. In order to stimulate different populations of LGN neurons with different receptive fields, six different orientations (0°, 30°, 60°, 90°, 120°, or 150°) of the gratings were used. Each orientation was presented for 3 s in pseudorandom order, such that all orientations were present in each 18 s block.

The M stimulus was a 100% luminance contrast black-white grating. The spatial frequency was 0.5 cycles per degree (cpd), and the temporal frequency was 15 Hz. The P stimulus was a red-green grating with minimal luminance contrast. The spatial frequency of the P stimulus was 2 cpd, and the temporal frequency was 5 Hz. The red and green levels of the P stimulus were the same as those used in Denison et al., 2014, where they were selected using flicker photometry. The blank stimulus was a grey screen of mean luminance.

Fifteen 18-second blocks were presented on each run (6 M, 6 P, and 3 blank). The blocks were presented in pseudorandom order with the constraint that two blocks of the same stimulus type could not appear consecutively, thereby minimizing neural adaptation to the stimuli. A white fixation point subtending 0.2° of visual angle was presented at the center of the screen. Subjects were instructed to maintain fixation throughout the run.

Previous work from our group has shown that spatial attention increases SNR of fMRI responses (Bressler and Silver, 2010; Bressler et al., 2020). We therefore had subjects perform a target detection task (Fig. 1B) during the M and P stimulus blocks, encouraging them to attend to the visual stimuli for the duration of the run. Targets were contrast decrements in the shape of 2D Gaussians, presented for 300 ms. Luminance

contrast decrements were used for the M blocks and color contrast decrements for the P blocks (since luminance contrast was already minimal for the latter). To make task difficulty (and attention demands) similar across the stimulus, the target size (the sigma parameter of the Gaussian constrast decrement) scaled linearly with eccentricity. Target size was set separately for the M and P conditions for each subject to approximately equate the difficulty of the M and P conditions. Average accuracy was 78.8% ± 5.2% for the M condition and 72.3% ± 6.1% for the P condition. These values are significantly above chance (25%) and below ceiling performance.

During each M and P block, 0-3 targets appeared on the screen, and subjects were asked to count the number in each block. The timing and location of the targets was random. A response period of 1.75 s followed each 18 s block, during which the screen turned grey, and the fixation point turned black. During this time, subjects indicated via button press how many targets they saw during the previous block. After the response period, the fixation point turned white for 500 ms, indicating the onset of the subsequent block. Including stimulus, response, and cue periods, each block was 20.25 s (9 TR) long. A 9 second (4 TR) blank period was presented at the beginning of each run. M/P localizer runs were about 5 minutes in length, with 8-10 (median 8) collected per session.

Population receptive field retinotopic mapping of cortex

We used an updated version of the pRF mapping procedure described in Sheremata and Silver (2015). Stimuli for the pRF mapping sessions consisted of a naturalistic scene presented within a drifting bar that traversed a circular aperture of diameter 28° of visual angle (Fig. 1C). This bar subtended 4° of visual angle and moved across the aperture at 8 different orientations equally spaced 45° apart (0°, 45°, 90°, …, 315°). The duration of each sweep of the drifting bar was 16 sec, the velocity was 2° of visual angle/sec, and there were two sweeps per orientation. Subjects were instructed to maintain fixation for the duration of the session. Each pRF run lasted approximately five minutes. Twelve runs were collected per session, yielding about an hour of BOLD data. All subjects participated in four sessions of pRF mapping. These sessions included spatial attention and cholinergic pharmacological manipulations that will be reported elsewhere. For the purposes of the present study, the pRF data were only used to define the boundaries of topographic cortical areas, and data were pooled across all attention and pharmacological (5 mg of the cholinesterase inhibitor donepezil or placebo) conditions.

Coupling between M and P LGN subdivisions and identified cortical areas

Steady-state coupling between M and P LGN subdivisions and cortical visual areas was evaluated using a modified version of the M/P localizer task. The same gratings were used as visual stimuli, but each 297-sec fMRI run was of only one stimulus type (M or P), and participants were instructed to press a button whenever they detected a contrast decrement target. This design minimized effects of stimulus transients on functional coupling measures. Participants were cued to attend to either the left or the right visual hemifield during each run. Whether to attend left or right was indicated before the task began and by the color of the fixation dot during the task. Average accuracy was 75.9% ± 1.8% and did not differ based on attended visual hemifield (L: 75.3% ± 1.8%, R: 76.6% ± 1.8%). Average accuracy was 82.2% ± 1.4% for the M condition and 69.7% ± 2.1% for the P condition. These values are significantly above chance (near zero accuracy) and below ceiling performance.

In each session of the coupling task, participants completed 8-12 (median: 12) runs of the coupling task. These were grouped in sets of four covering the two types of stimulus (M or P) and spatial attention (attend left or attend right) conditions. Two sessions of data were acquired for this task, resulting in 90-120 min of coupling fMRI data for each subject.

MRI data acquisition

All MRI data were acquired in the Henry H. Wheeler, Jr. Brain Imaging Center at the University of California, Berkeley, on a Siemens TIM/Trio 3 T MR scanner with a 32-channel RF head coil. Foam padding was placed around the head to minimize head motion. For two out of five subjects, a custom 3-D printed headcase was used instead of foam padding.

The same echo planar imaging (EPI) pulse sequence was used to acquire BOLD data in the LGN localization and functional coupling sessions. This T2*-weighted gradient-echo EPI sequence with 6/8 partial Fourier acquisition used multiband acceleration (Moeller et al., 2010) to acquire 3 slices simultaneously. A total of 69 slices (1.75 mm thick) were acquired with a 120 × 120 matrix and in-plane FOV of 210 × 210 mm, yielding an isotropic spatial resolution of 1.75 mm and covering the entire brain. Repetition time (TR) was 2250 ms, and 139 volumes were acquired on each run. Echo time (TE) was 32.8 ms, flip angle was 45°, the phase encoding direction was anterior-to-posterior, and echo spacing was 0.69 ms. A Siemens signal intensity normalization filter was applied at the time of acquisition to reduce spatial inhomogeneities. All subjects participated in one session of LGN localization and two sessions of coupling, each lasting approximately one hour.

For the population receptive field mapping sessions, BOLD data were acquired using the same sequence as in a previously described pRF mapping study (Sheremata and Silver, 2015). This gradient-echo EPI sequence had a TR of 2 s, a TE of 30 ms, flip angle = 80°, and a spatial resolution of 3 × 3 × 2.3 mm. Twenty-two slices were acquired at an angle of ~30° from the axial plane, providing coverage of occipital and posterior parietal cortex. Four sessions of approximately one hour each were collected for the cortical pRF mapping. During one of the pRF sessions, a high resolution (1 x 1 x 1 mm) T1-weighted anatomical scan was also collected.

Data Analysis

fMRI preprocessing

Preprocessing was implemented in Python using nipype (Esteban et al., 2022) and tools from the FMRIB Software Library (FSL; Jenkinson et al., 2012). For each functional run, a reference volume was calculated by taking the mean across all acquisitions in that run. The reference volume for the first functional run in each of the three sessions was selected as the reference volume for that session. All volumes of the functional runs in a session were then aligned to this reference volume using FSL MCFLIRT (Jenkinson et al., 2002).

Localizer data were then preprocessed for analysis. First, we discarded volumes at the beginning and end of the functional runs. For hemifield localizer runs, six volumes were discarded at the beginning, corresponding to one half of a stimulus alternation cycle. One volume was also trimmed from the end of the run, leaving 132 volumes for

the analysis, corresponding to the 297 seconds of visual stimulation in the hemifield localizer stimulus. For M/P localizer runs, four volumes were discarded from the beginning, leaving 135 volumes for analysis.

Alignment

For each subject and session, the reference BOLD volume was aligned to the high-resolution anatomical volume using FSL tools. The inverse of this transformation was also calculated, allowing cortical areas that were defined in the space of the high-resolution T1 anatomical image to be projected into the space of the functional data. By concatenating the transforms from one functional space to the anatomical space and from the anatomical space to a different set of functional data, regions of interest were transformed between functional spaces.

Estimation of responses via Generalized Linear Models (GLMs)

FSL was used to fit GLMs to the hemifield localizer and M/P localizer runs. In the hemifield localizer runs, the design matrix contained L and R regressors corresponding to stimulation of the left and right visual hemifields. These had a value of 1 when a given hemifield was being stimulated and 0 otherwise. For the M/P localizer runs, M and P regressors had a value of 1 when that stimulus type was presented and a value of 0 otherwise. Regressors were then convolved with a gamma function HRF to generate the final design matrix.

GLMs were fit to voxel timeseries from individual ~5-min runs, then parameter estimates were combined into a second-level estimate that used all runs from that session. This was done using FSL tools (FILM and FEAT especially). The outputs of this procedure were estimates of each voxel's response to L/R and M/P stimulation, hereafter referred to as beta values (e.g., betaM for a voxel's estimated response to M stimulation). The difference between betaL and betaR was used to measure the spatial selectivity of responses to visual stimuli in the two hemifields. Similarly, the difference between betaM and betaP quantified each voxel's relative response to M vs. P stimuli.

LGN ROI definition

Regions of interest (ROIs) were defined for the entire LGN (including both M and P subregions) by identifying clusters of voxels in the appropriate anatomical location that responded to contralateral visual stimulation, based on the difference between betaL and betaR values derived from the hemifield localizer runs. ROI borders were manually drawn around these voxels in functional space for each participant.

Subsequently, these LGN ROIs were subdivided into M and P subregions on the basis of each voxel's estimated response to M- vs P-type stimulation. Following the procedure described in Denison et al., 2014, the differences between betaM and betaP values were used to assign voxels to M (top 20%) or P (bottom 80%). These proportions were selected based on histological evidence that indicates an average of 20% of the volume of the LGN consists of the M layers and 80% by the P layers (Andrews et al., 1997; Selemon and Begovic, 2007).

pRF Estimation

Predicted fMRI timeseries were generated by convolving the spatioatemporal stimulus sequence with a 2-D Gaussian centered at different visual field locations

(Dumoulin and Wandell, 2008). The pRF for each voxel was defined as the center (x_0, y_0) and size (σ) of Gaussian that minimized the mean squared error between this predicted timeseries and the observed voxel timeseries.

Expressing the receptive field centers in polar coordinates results in maps of preferred eccentricity and polar angle for each voxel. Cortical visual areas were then defined based on the distribution of pRF centers along the cortical surface and the pattern of reversals in adjuacent pairs of polar angle maps with shared visual field meridian representations (see Wandell, Dumoulin, and Brewer, 2007). Specifically, we sought to define V1, V2d/v, V3d/v, V3A/B, V4, IPS0-5, LO1/2, VO1/2, and TO1/2.

Regions with separate dorsal and ventral hemifield representations like V2 and V3 were combined into regions that had a full contralateral representation. Additionally, V3A and V3B were defined separately in some subjects but not others, so a larger area V3A/B was defined as the union of both V3A and V3B if separately defined, or the single V3A/B area if not. All IPS0-5 areas that could be defined were combined into a single IPS area. Similarly, LO1/2 were combined into LO, TO1/2 into TO, and VO1/2 into VO.

Organization of cortical areas into dorsal and ventral

In macaques, the dorsal stream runs from V1 through visual areas V2, V3, and V3A/B to parietal cortex and includes TO1 and TO2, the likely human homologs of macaque area MT and MST. The ventral stream runs from V1 through V2, V3, V4, and VO1/2 and include LO1 and LO2. (Wandell, Dumoulin, and Brewer, 2007). For this study, we labeled areas V1, V2, and V3 early, V3A/B and IPS as dorsal, and V4 and VO1/2 as ventral.

Coupling analysis

First, timeseries were bandpass filtered between 0.02 and 0.15 Hz. Next, thalamocortical coupling was estimated using a coherence-based approach implemented in Python and using nitime (Rokem, Trumpis, and Perez, 2008). Specifically, we performed a seed coherence analysis with 64 frequency bins to estimate the strength of coupling between one of the subdivisions of the LGN and an individual cortical area. Regions of interest in the LGN were transformed from the space of the M/P localizer session to that of the coupling session, resulting in a probabilistic mask in the space of the coupling data. We imposed a volume constraint by using the same number of voxels from within the probabilistic mask as were in the ROI in the original functional space. Since the voxel size was identical in the two sessions, this was equivalent to a requirement that a given LGN ROI has the same volume across sessions.

The mean of all voxel timeseries from the LGN region was used as the seed timeseries for all coherence analyses. Once the seed timeseries was computed, coherence was estimated with each of the voxel timeseries in the target cortical areas. Subsequently, coherence measurements were averaged across all voxels in the cortical areas to provide a single measure of thalamocortical coupling per LGN - cortical area pair.

3.3 Results

LGN Localizers

We used GLMs to model the data from both the hemifield and M/P localizer tasks as described in the Methods section ("Estimation of responses via Generalized Linear Models"). Analysis of the hemifield localizer data yielded clusters of voxels at the appropriate anatomical locations with high contralateral spatial selectivity of visual responses (difference between betaL and betaR values). LGN ROI boundaries were drawn over these clusters. Subsequently, a GLM analysis contrasting M and P blocks of the M/P localizer task (betaM- betaP values) revealed contiguous clusters of M and P voxels in the appropriate anatomical locations within the functionally-defined LGNs. These findings constitute a replication of the procedure described in Denison et al. (2014) for identifying the locations of the magnocellular and parvocellular subregions of the LGN.

We additionally analyzed the spatial distribution of the M and P voxels in the LGN (Fig. 2). Specifically, we calculated centers of mass (COMs) of the M and P regions and evaluated whether these matched the known anatomical relations, in which the M layers of the LGN are more ventromedial than the P layers. We found that this was the case, consistent with histological studies as well as the results of Denison et al. (2014).

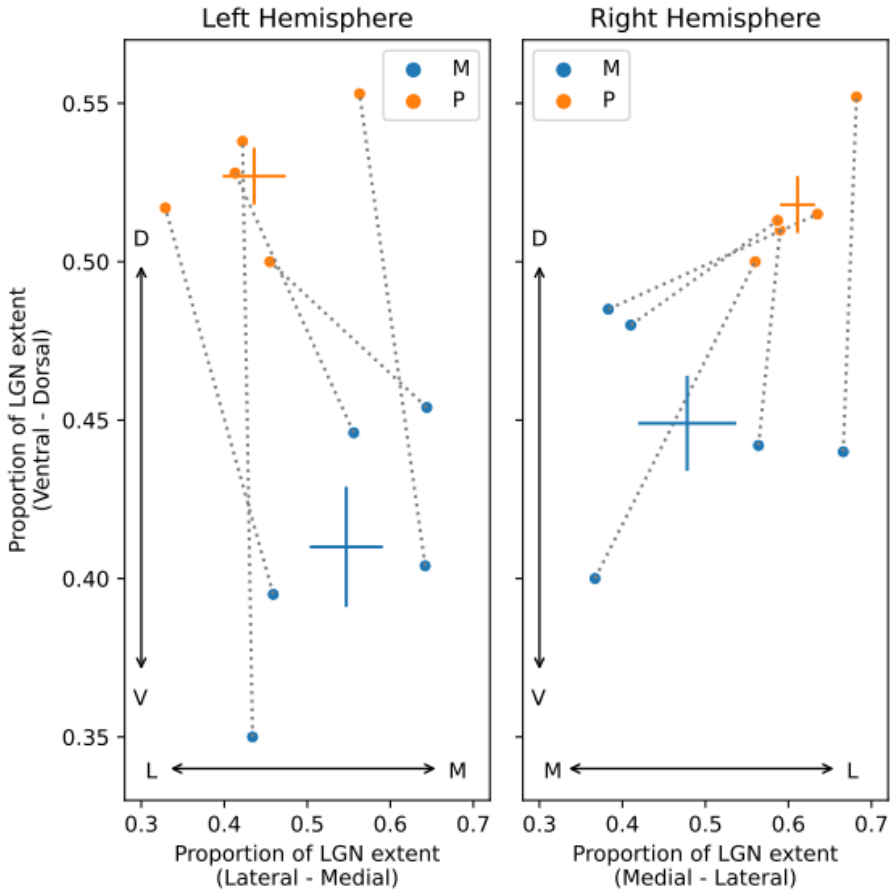

Figure 2. Center of Mass analysis. For both hemispheres, the functionally defined M region was more ventral and more medial than the P region. All four of these differences were significant before and after false discovery rate correction.

We tested whether the M COMs were more ventral and more medial than the P COMs separately for both the left and right LGNs. This procedure resulted in a total of four t-tests, all one-tailed. All four tests were significant both before and after correction for multiple comparisons using false discovery rate correction (Benjamini and Hochberg, 1995). For the left LGN, the M subdivision was more ventral ($p = 0.005$) and more medial ($p = 0.011$) than the P subdivision, and the same pattern was observed in the right LGN (ventral $p = 0.007$, medial $p = 0.024$).

A major difference between our study and Denison et al., 2014 was that we used multiband acquisition (acceleration factor: 3) to record from the entire brain at once (Moeller et al., 2010). Without the multiband acquisition (and keeping all other acquisition parameters the same), the recorded brain volume would have been 3.675 cm in the narrowest dimension, and it would be have been impossible to include both dorsal and ventral stream cortical areas as well as the LGN. Our results extend the procedure described in Denison et al., 2014 to multi-band acquisitions.

M/P Coupling

We estimated thalamocortical coupling between either M or P LGN subdivisions and all identified cortical visual areas as described in the Methods section under

"Coupling Analysis". This calculation was performed separately for each hemisphere, then results from the left and right hemispheres were averaged. We then compared these coherence values for a given LGN subdivision – cortical area pair under either M-type or P-type stimulation. Critically, this comparison involved the exact same seed and target voxels, with only the type of visual stimulation differing between the two conditions. We hypothesized that the M subdivision of the LGN would show higher coupling with cortical visual areas under compatible (M-type) stimulation than under incompatible (P-type) stimulation. Analogously, we expected the P subdivision of the LGN to have higher coupling to cortical visual areas under compatible (P-type) stimulation than incompatible (M-type) stimulation. However, there were no significant differences in coherence for M-type and P-type stimulation for any LGN subdivision/cortical pairing (Figure 3). Because voxels were selected from a probabilistic mask, we also tried weighting each voxel by the square of these probabilities to emphasize signal from more certain voxels, but this did not alter the pattern of results.

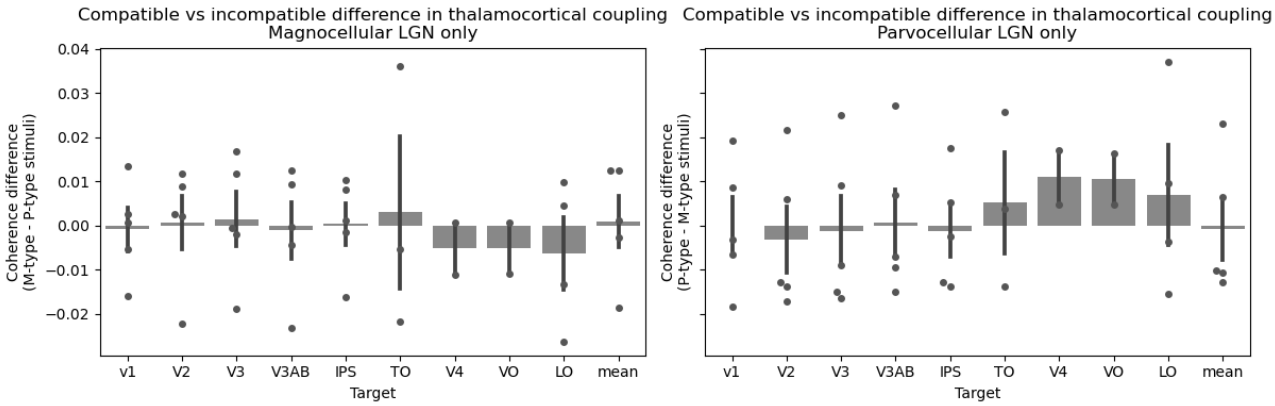

Figure 3. Compatible vs. incompatible coupling results for the magno- and parvocellular LGN subregions and ipsilateral cortical visual areas. Black circles represent individual participants. Left: M LGN. Right: P LGN. The rightmost bar indicates the mean coherence difference across all cortical areas defined for each subject. No significant effects were observed in either analysis.

Next, we summed the differences shown in Figure 3 for M and P LGNs for each subject to create a single measure of the effect of stimulus type on thalamocortical coupling. Positive values of this metric indicate that coupling of a given LGN subdivision (M or P) with a given cortical area was greater when the compatible type of visual stimulus (M-type or P-type) was presented, compared to coherence values for the same voxels when the incompatible type of stimulus was presented. A value of zero indicates that stimulus type had no overall effect on (M or P) LGN coherence with a given cortical region. The values were not significantly different from zero for any LGN/cortical area pair (Figure 4, left).

We repeated this analysis using subsets of LGN voxels that were most clearly classified as either M or P, while preserving the relative sizes of the M and P areas. Specifically, we used the tails of the distribution of the difference of betaM and betaP values for each LGN (the 40% most P and 10% most M voxels). The purpose of this analysis was to exclude voxels with more ambiguous differential responses to M and P stimuli, whether due to partial voluming, vascular artifacts, or other sources of noise. We

also found no evidence for modulation of LGN/cortical coupling by stimulus type for these more restricted ROIs (Figure 4, right).

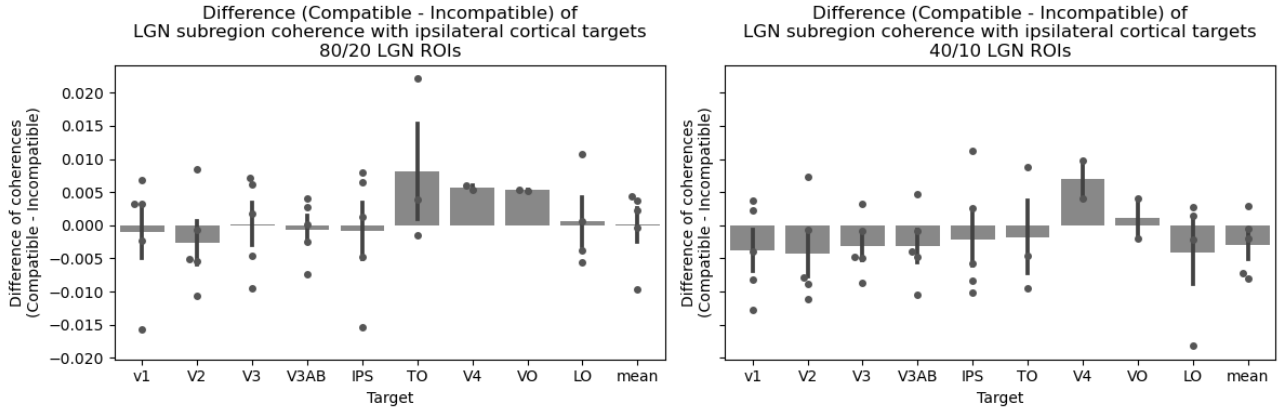

Figure 4. Compatible vs. incompatible coupling results combined across magno- and parvocellular LGNs. Left: 80P/20M ROIs. Right: 40P/10M ROIs. Black circles represent individual participants. The rightmost bar indicates the mean coherence difference across all cortical areas defined for each subject. No significant effects were observed in either analysis.

Spatial Attention effects

We analyzed the effects of spatial attention on thalamocortical coupling using estimates of the coherence between the entire LGN (combined M and P subdivisions) and individual ipsilateral visual cortical regions. Because each hemisphere of the brain represents contralateral visual information, we were able to compare coupling between the exact same set of voxels in the LGN (seed) and cortical visual areas (targets) when a given visual hemifield was being attended or ignored (with attention directed to the opposite hemifield). For example, we expected higher coherence values between the right LGN and individual visual cortical regions in the right hemisphere when participants attended to the left visual hemifield compared to when they attended to the right visual hemifield.

We did not find a significant effect of spatial attention on coupling between the whole LGN and the identified visual cortical areas (Fig. 5). Significant effects were found for a small number of cortical areas under quadratic weighting of included LGN voxels, but these findings were not robust to different choices of analysis parameters, and would not have survived correction for multiple comparisons even if they were. We also measure attentional modulation of thalamocortical connectivity separately for the M and P subregions of the LGN, but again found no significant effects of spatial attention.

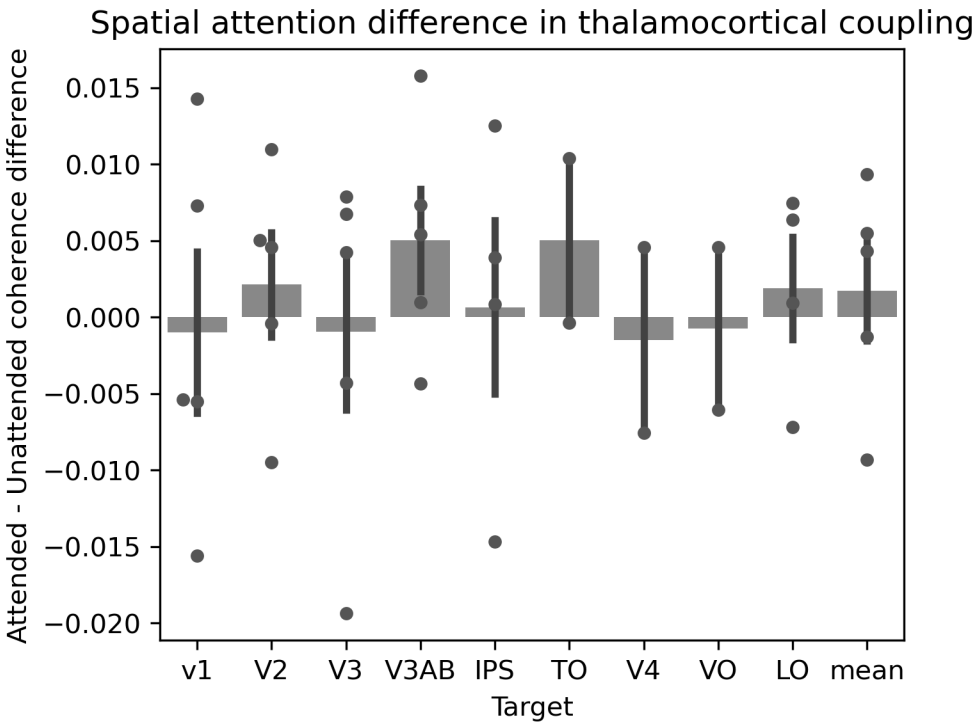

Figure 5. There were no significant effects of spatial attention on coupling between the entire LGN and ipsilateral cortical regions.

3.4 Discussion

We used coherence to quantify coupling between individual subdivisions of the LGN (magnocellular or parvocellular) and topographically-organized visual cortical areas in the dorsal and ventral cortical processing streams. The primary goal of this study was to test whether there was preferential functional coupling between the M subdivision of the LGN and dorsal cortical regions and between the P subdivision of the LGN and ventral cortical regions (Livingstone and Hubel, 1984). However, we were unable to detect any differences in functional coupling between M or P subdivisions of the LGN and any cortical region for stimuli optimized to preferentially drive either the M or the P system. Given this, our data cannot address the hypothesis that the M subdivision of the LGN is preferentially coupled with dorsal cortical regions and that the P subdivision of the LGN is preferentially coupled with ventral cortical region.

Our results demonstrate that the procedure described in Denison et al. (2014) reliably localized the M and P subdivisions of the LGN at 3T base magnetic field strength and with multiband acuqisition. In particular, the M/P localizer task consistently resultd in differential activation of the corresponding subregions of the LGN.

We avoided circularity by defining our regions of interest in the LGN and then measuring coupling of these LGN subdivisions with cortical regions in independent data sets. Specifically, we defined the LGN based on the hemifield localizer, then defined the M/P regions based on the M/P localizer, and defined cortical visual areas based on the

pRF mapping sessions. We then collected separate data sets on a different day to evaluate functional coupling.

One possible reason for our lack of significant coupling results is inaccuracy in inter-session alignment of functional data. The subdivisions of the LGN are very small (about 100 mm3 for the M subdivision and 400 mm3 for the P subdivision) and adjacent to each other, and an entire session was devoted to mapping them in each participant. These defined regions of interest were then aligned with data from a separate session in which functional coupling data were acquired. Small errors in alignment could have resulted in misassignment of voxels in the M and P subdivisions of the LGN.

Poor SNR in the LGN could also have contributed to the lack of significant functional coupling results. It is possible that using higher base field strength MRI (such as 7T instead of 3T) could have enhanced sensitivity for detecting effects of stimulus type of attention on coupling between LGN subdivisions and cortical regions. As shown in Denison et al. (2014), the advantages of 7T compared to 3T include better SNR in the LGN even for similar voxel sizes. In addition, 7T scanners could be used to improve spatial resolution, thereby reducing partial voluming effects and allowing for more reliable definition of small subcortical areas. More recent work (Qian et al., 2020) has succeeded in differentially activating and mapping the M and P LGN subregions at 7T with good inter-session reliability.

Another contributing factor to our lack of significant coupling results may have been the use of multi-band acquisitions. The ability to acquire multiple slices per TR allowed us to record from the entire brain, but multiband acquisition has recently been shown to reduce SNR in regions near the center of the brain (Srirangarajan et al., 2021). Reduced SNR in the LGN with multiband acquisition may have limited sensitivity for measuring changes in functional coupling with the cortex.

Another possibility is that the design of our coupling task was not optimal for measuring functional coupling. In our study, each run was approximately 5 minutes long, but the reliability of functional connectivity results is improved for continuous acquisitions of 9-12 min (Birn et al., 2013). However, some subjects reported that continuous viewing of the large, contrast reversing stimuli in our study was quite intense (particularly the 100% luminance contrast M stimulus), so increasing the length of the runs might have led to subject attrition.

In conclusion, we successfully identified the M and P LGN subdivisions, replicating the M/P findings described in Denison et al., 2014 and extending them to fMRI data acquired with multiband acceleration. However, we failed to detect any differences in functional coupling between these LGN subdivisions and cortical visual areas due to stimulus type or attention. We suggest that a future study at higher magnetic field strength and finer spatial resolution would permit the detection of these effects.

3.5 Acknowledgements

This research was funded by the National Eye Institute at the National Institutes of Health (R21 EY023091 to M.A.S., R01 EY025278 to M.A.S., and Core Grant for Vision Research P30 EY003176) and the National Science Foundation (Major Instrumentation Program Grant BCS-0821855).

3.6 References

Amano, K., Wandell, B. A., and Dumoulin, S. O. (2009). Visual Field Maps, Population Receptive Field Sizes, and Visual Field Coverage in the Human MT+ Complex. J Neurophysiol 102, 2704–2718. doi: 10.1152/jn.00102.2009.

Andrews, T. J., Halpern, S. D., and Purves, D. (1997). Correlated Size Variations in Human Visual Cortex, Lateral Geniculate Nucleus, and Optic Tract. J Neurosci 17, 2859–2868. doi: 10.1523/JNEUROSCI.17-08-02859.1997.

Benjamini, Y., and Hochberg, Y. (1995). Controlling the False Discovery Rate: A Practical and Powerful Approach to Multiple Testing. Journal of the Royal Statistical Society. Series B (Methodological) 57, 289–300.

Birn, R. M., Molloy, E. K., Patriat, R., Parker, T., Meier, T. B., Kirk, G. R., et al. (2013). The effect of scan length on the reliability of resting-state fMRI connectivity estimates. Neuroimage 83, 550–558. doi: 10.1016/j.neuroimage.2013.05.099.

Braddick, O. J., O'Brien, J. M. D., Wattam-Bell, J., Atkinson, J., Hartley, T., and Turner, R. (2001). Brain Areas Sensitive to Coherent Visual Motion. Perception 30, 61–72. doi: 10.1068/p3048.

Brainard, D. H. (1997). The Psychophysics Toolbox. Spatial Vision 10, 433–436. doi: 10.1163/156856897X00357.

Bressler, D. W., and Silver, M. A. (2010). Spatial attention improves reliability of fMRI retinotopic mapping signals in occipital and parietal cortex. Neuroimage 53, 526–533. doi: 10.1016/j.neuroimage.2010.06.063.

Bressler, S. L., Tang, W., Sylvester, C. M., Shulman, G. L., and Corbetta, M. (2008). Top-Down Control of Human Visual Cortex by Frontal and Parietal Cortex in Anticipatory Visual Spatial Attention. J Neurosci 28, 10056–10061. doi: 10.1523/JNEUROSCI.1776-08.2008.

Denison, R. N., Vu, A. T., Yacoub, E., Feinberg, D. A., and Silver, M. A. (2014). Functional mapping of the magnocellular and parvocellular subdivisions of human LGN. Neuroimage 102, 358–369. doi: 10.1016/j.neuroimage.2014.07.019.

Dumoulin, S. O., and Wandell, B. A. (2008). Population receptive field estimates in human visual cortex. NeuroImage 39, 647–660. doi: 10.1016/j.neuroimage.2007.09.034.

Esteban, O., Markiewicz, C. J., Burns, C., Goncalves, M., Jarecka, D., Ziegler, E., et al. (2022). nipy/nipype: 1.8.3. doi: 10.5281/zenodo.6834519.

Felleman, D. J., and Van Essen, D. C. (1991). Distributed Hierarchical Processing in the Primate Cerebral Cortex. Cerebral Cortex 1, 1–47. doi: 10.1093/cercor/1.1.1.

Gaffan, D., Harrison, S., and Gaffan, E. (1986). Visual identification following inferotemporal ablation in the monkey. The Quarterly journal of experimental psychology. B, Comparative and physiological psychology 38. Available at: https://pubmed.ncbi.nlm.nih.gov/3704185/ [Accessed November 3, 2022].

Gandhi, S. P., Heeger, D. J., and Boynton, G. M. (1999). Spatial attention affects brain activity in human primary visual cortex. Proc Natl Acad Sci U S A 96, 3314–3319. doi: 10.1073/pnas.96.6.3314.

Goodale, M. A., Meenan, J. P., Bülthoff, H. H., Nicolle, D. A., Murphy, K. J., and Racicot, C. I. (1994). Separate neural pathways for the visual analysis of object shape in perception and prehension. Current Biology 4, 604–610. doi: 10.1016/S0960-9822(00)00132-9.

Grill-Spector, K., Weiner, K. S., Kay, K., and Gomez, J. (2017). The Functional Neuroanatomy of Human Face Perception. Annu Rev Vis Sci 3, 167–196. doi: 10.1146/annurev-vision-102016-061214.

Hubel, D. H., and Livingstone, M. S. (1990). Color and contrast sensitivity in the lateral geniculate body and primary visual cortex of the macaque monkey. J Neurosci 10, 2223–2237. doi: 10.1523/JNEUROSCI.10-07-02223.1990.

Jenkinson, M., Bannister, P., Brady, M., and Smith, S. (2002). Improved optimization for the robust and accurate linear registration and motion correction of brain images. Neuroimage 17, 825–841. doi: 10.1016/s1053-8119(02)91132-8.

Jenkinson, M., Beckmann, C. F., Behrens, T. E. J., Woolrich, M. W., and Smith, S. M. (2012). FSL. NeuroImage 62, 782–790. doi: 10.1016/j.neuroimage.2011.09.015.

Jones, E. G. (1986). The Thalamus. New York: Plenum Press Available at: https://link.springer.com/book/10.1007/978-1-4615-1749-8 [Accessed November 3, 2022].

Kastner, S., Schneider, K. A., and Wunderlich, K. (2006). "Chapter 8 Beyond a relay nucleus: neuroimaging views on the human LGN," in Progress in Brain Research (Elsevier), 125–143. doi: 10.1016/S0079-6123(06)55008-3.

Lauritzen, T. Z., D'Esposito, M., Heeger, D. J., and Silver, M. A. (2009). Top–down flow of visual spatial attention signals from parietal to occipital cortex. Journal of Vision 9, 18. doi: 10.1167/9.13.18.

Livingstone, M. S., and Hubel, D. H. (1984). Anatomy and physiology of a color system in the primate visual cortex. J. Neurosci. 4, 309–356. doi: 10.1523/JNEUROSCI.04-01-00309.1984.

Merigan, W. H., and Maunsell, J. H. (1993). How parallel are the primate visual pathways? Annu Rev Neurosci 16, 369–402. doi: 10.1146/annurev.ne.16.030193.002101.

Mishkin, M., and Ungerleider, L. G. (1982). Contribution of striate inputs to the visuospatial functions of parieto-preoccipital cortex in monkeys. Behavioural Brain Research 6, 57–77. doi: 10.1016/0166-4328(82)90081-X.

Moeller, S., Yacoub, E., Olman, C. A., Auerbach, E., Strupp, J., Harel, N., et al. (2010). Multiband multislice GE-EPI at 7 tesla, with 16-fold acceleration using partial parallel imaging with application to high spatial and temporal whole-brain fMRI. Magnetic Resonance in Medicine 63, 1144–1153. doi: 10.1002/mrm.22361.

O'Connor, D. H., Fukui, M. M., Pinsk, M. A., and Kastner, S. (2002). Attention modulates responses in the human lateral geniculate nucleus. Nat Neurosci 5, 1203–1209. doi: 10.1038/nn957.

Orban, G. A., Van Essen, D., and Vanduffel, W. (2004). Comparative mapping of higher visual areas in monkeys and humans. Trends in Cognitive Sciences 8, 315–324. doi: 10.1016/j.tics.2004.05.009.

Peirce, J., Gray, J. R., Simpson, S., MacAskill, M., Höchenberger, R., Sogo, H., et al. (2019). PsychoPy2: Experiments in behavior made easy. Behav Res 51, 195–203. doi: 10.3758/s13428-018-01193-y.

Pelli, D. G. (1997). The VideoToolbox software for visual psychophysics: transforming numbers into movies. Spatial Vision 10, 437–442. doi: 10.1163/156856897X00366.

Qian, Y., Zou, J., Zhang, Z., An, J., Zuo, Z., Zhuo, Y., et al. (2020). Robust functional mapping of layer-selective responses in human lateral geniculate nucleus with high-resolution 7T fMRI. Proceedings of the Royal Society B: Biological Sciences 287, 20200245. doi: 10.1098/rspb.2020.0245.

Rokem, A., Trumpis, M., and Pèrez, F. (2009). Nitime: time-series analysis for neuroimaging data. in 8th Python in Science Conference (SciPy).

Schneider, K. A., and Kastner, S. (2009). Effects of Sustained Spatial Attention in the Human Lateral Geniculate Nucleus and Superior Colliculus. J. Neurosci. 29, 1784–1795. doi: 10.1523/JNEUROSCI.4452-08.2009.

Selemon, L. D., and Begović, A. (2007). Stereologic analysis of the lateral geniculate nucleus of the thalamus in normal and schizophrenic subjects. Psychiatry Res 151, 1–10. doi: 10.1016/j.psychres.2006.11.003.

Sheremata, S. L., and Silver, M. A. (2015). Hemisphere-Dependent Attentional Modulation of Human Parietal Visual Field Representations. J. Neurosci. 35, 508–517. doi: 10.1523/JNEUROSCI.2378-14.2015.

Sherman, S. M., and Guillery, R. W. (2001). Exploring the Thalamus - 1st Edition. San Diego: Academic Press Available at: https://www.elsevier.com/books/exploring-the-thalamus/sherman/978-0-12-305460-9 [Accessed November 4, 2022].

Sherman, S. M., and Guillery, R. W. (2002). The role of the thalamus in the flow of information to the cortex. Philos Trans R Soc Lond B Biol Sci 357, 1695–1708. doi: 10.1098/rstb.2002.1161.

Silver, M. A., and Kastner, S. (2009). Topographic maps in human frontal and parietal cortex. Trends in Cognitive Sciences 13, 488–495. doi: 10.1016/j.tics.2009.08.005.

Silver, M. A., Ress, D., and Heeger, D. J. (2005). Topographic Maps of Visual Spatial Attention in Human Parietal Cortex. Journal of Neurophysiology 94, 1358–1371. doi: 10.1152/jn.01316.2004.

Silver, M. A., Ress, D., and Heeger, D. J. (2007). Neural Correlates of Sustained Spatial Attention in Human Early Visual Cortex. Journal of Neurophysiology 97, 229–237. doi: 10.1152/jn.00677.2006.

Smith, A. M., Lewis, B. K., Ruttimann, U. E., Ye, F. Q., Sinnwell, T. M., Yang, Y., et al. (1999). Investigation of Low Frequency Drift in fMRI Signal. NeuroImage 9, 526–533. doi: 10.1006/nimg.1999.0435.

Srirangarajan, T., Mortazavi, L., Bortolini, T., Moll, J., and Knutson, B. (2021). Multi-band FMRI compromises detection of mesolimbic reward responses. NeuroImage 244, 118617. doi: 10.1016/j.neuroimage.2021.118617.

Sun, F. T., Miller, L. M., and D'Esposito, M. (2004). Measuring interregional functional connectivity using coherence and partial coherence analyses of fMRI data. NeuroImage 21, 647–658. doi: 10.1016/j.neuroimage.2003.09.056.

Ungerleider, L. G., and Haxby, J. V. (1994). 'What' and 'where' in the human brain. Current Opinion in Neurobiology 4, 157–165. doi: 10.1016/0959-4388(94)90066-3.

Wandell, B. A., Dumoulin, S. O., and Brewer, A. A. (2007). Visual Field Maps in Human Cortex. Neuron 56, 366–383. doi: 10.1016/j.neuron.2007.10.012.

Wiesel, T. N., and Hubel, D. H. (1966). Spatial and chromatic interactions in the lateral geniculate body of the rhesus monkey. Journal of Neurophysiology 29, 1115–1156. doi: 10.1152/jn.1966.29.6.1115.

4 Conclusion

The results of these studies advance our understanding of the relationship between brain function and perceptual outcomes in humans. In Chapter 2, we show a negative correlation between the depth of amblyopia (interocular difference in visual acuity) and visual cortical GABA concentration that was not observed in a sensorimotor cortical control region (Mukerji et al., 2022). In addition, we found opposite correlations between dichoptic interocular surround suppression and visual cortical GABA levels for the two eyes of persons with amblyopia, for both cross- and iso-oriented surrounds.

In Chapter 3, we show that the magnocellular and parvocellular subdivisions of the LGN can be localized using fMRI, and that this procedure works when combined with multiband imaging to record from the entire brain. Surprisingly, we did not find any differential functional coupling between these LGN subdivisions and visual cortical areas due to stimulus type or attention. However, the power of non-invasive techniques for functionally localizing and recording from small structures deep in the brain remains attractive. We conjecture that a future study using more recent developments in fMRI (e.g., Feinberg, Vu, and Beckett, 2018) to achieve much higher resolution would yield even richer insights into the relationship between the structure and function of the human visual system.

4.1 References

Feinberg, D. A., Vu, A. T., and Beckett, A. (2018). Pushing the limits of ultra-high resolution human brain imaging with SMS-EPI demonstrated for columnar level fMRI. NeuroImage 164, 155–163.

Mukerji, A., Byrne, K. N., Yang, E., Levi, D. M., and Silver, M. A. (2022). Visual cortical γ−aminobutyric acid and perceptual suppression in amblyopia. Frontiers in Human Neuroscience 16.